SINTEF Energy Research

Master's Thesis – PFE-Master

Numerical and mathematical analysis of a five-equation model for two-phase flow

Author
Pedro José Martínez Ferrer

Supervisors
Svend Tollak Munkejord
Tore Flåtten

April 12, 2010 - October 12, 2010

Summary

We study a two-phase pipe flow model with relaxation terms in the energy equations, driving the model towards thermal equilibrium. This equilibrium state is characterized by the temperatures being equal in each phase.

We then derive a linearized approximate Riemann solver satisfying the Roe conditions for the thermally relaxed model, i.e. the model with equal temperatures but unequal velocities in each phase. Using standard high-resolution techniques approximating second-order accuracy for smooth solutions, we compare this model to a fully non-relaxed model through numerical experiments. Our simulations indicate that thermal relaxation in the two-fluid model has negligible impact on mass transport dynamics. However, the velocity difference of sonic propagation in the thermally relaxed and unrelaxed two-fluid model may significantly affect practical simulations.

Preface

The present work constitutes the Master's Thesis for the double degree of engineer at ENSMA (Ecole Nationale Supérieure de Mécanique et d'Aérotechnique) and ETSIA (Escuela Técnica Superior de Ingenieros Aeronáuticos) Universities.

This Thesis has been realised in SINTEF Energy Research, located in Trondheim, Norway. The financial support received from SINTEF, as well as the grant received from the French government are gratefully acknowledged.

I would like to give my sincere gratitude to my supervisors, Svend Tollak Munkejord and Tore Flåtten, for their helpful guidances and valuable discussions which aided me along the work.

Finally, I would like to thank all my colleagues at office, and all the people I have had the opportunity to meet with in Norway, for the enjoyable time I spent with them and for making of my stay in Norway a beautiful and unrepeatable experience.

Pedro José Martínez Ferrer.
Trondheim, October 2010.

Contents

List of Figures

List of Tables

Nomenclature

Abbrevations

CFL Courant-Friedrichs-Lewy

EOS Equation of state

LxF Lax-Friedrichs scheme

MC Monotonized central difference

MUSCL Monotone upwind-centred scheme for conservation laws (higher-order extension of MUSTA scheme)

MUSTA Multi-stage scheme

Greek letters

α	Volume fraction	-
β	Wave strength	-
χ	Parameter vector	-
δ	Parameter in the smoothed absolute-value function	-
γ	Ratio of specific heats	-
λ	Eigenvalue	m/s
Λ	Diagonal matrix containing eigenvalues	m/s
ϕ_δ	Smoothed absolute-value function	-
ρ	Density	kg/m^3
σ	Parameter related to the pressure jump at the gas-liquid interface	-

Latin letters

A	Jacobian matrix	-
$\hat{A}$	Roe matrix	-
B	Coefficient matrix of nonconservative terms	-

c	Speed of sound	m/s
c_p	Specific heat at constant pressure	J/kg
c_v	Specific heat at constant volume	J/kg
$\mathcal{C}$	Cell grid	-
e	Internal energy	$(\mathrm{m/s})^2$
E	Total energy	$\mathrm{kg/(m\,s^2)}$
$\mathscr{E}$	Maximum relative error in the pressure	-
F	Flux vector	-
$\hat{F}$	High-resolution correction flux vector	-
g	Gravitational acceleration	$\mathrm{m/s^2}$
H	Total enthalpy	$(\mathrm{m/s})^2$
I	Volumetric momentum, $I_k = \rho_k \alpha_k v_k$	$\mathrm{kg/(m^2\,s)}$
m	Volumetric mass, $m_k = \rho_k \alpha_k$	$\mathrm{kg/m^3}$
p	Pressure	Pa
r	Right eigenvector	-
R	Matrix containing right eigenvectors as its columns	-
$\mathcal{R}$	Universal Gas Constant	J/(mol K)
s	Specific entropy	J/(kg K)
S	Source-term vector for composite variables	-
t	Time	s
T	Temperature	K
U	Vector containing the composite variables	-
U_i^n	Numerical approximation to the cell average of $U(x(i), t_n)$	-
v	Velocity	m/s
V	Volume	$\mathrm{m^3}$
W	Vector of nonconservative terms	-
$\mathcal{W}$	Wave	-
$\widehat{\mathcal{W}}$	Limited wave	-
x	Length coordinate	m

Other symbols

$\overline{\psi}$	Arithmetic mean value
$\overline{\overline{\psi}}$	Average over a formally consistent path
$\tilde{\psi}$	Geometric mean value
$\hat{\psi}$	Roe average
$\Delta\psi$	Jump

Subscripts

g	Gas
∞	Initial/Reference
i	Spatial index
k	Pertaining to phase k
l	Liquid
n	Time-step index
$*$	Initial/Reference

Superscripts

L	Left-hand side
n	Time-step index
p	Related to the pth eigenvalue
R	Right-hand side
0	Initial/Reference

Chapter 1

Introduction

The SINTEF Group is the largest independent research organisation in Scandinavia. SINTEF has approximately 2000 employees and its head office is in Trondheim. The SINTEF Group is organized in several research divisions, which have been defined in terms of value chains and industrial market clusters.

The SINTEF Energy Research is focused on finding solutions related to power production and conversion, transmission and distribution covering all the key areas from the indoor climate and energy used in buildings such as gas technology, combustion, bioenergy, refrigeration engineering and technology for the food and nutrition industry.

Two-phase flows, and in general multiphase flows, are important in a large range of industrial applications, such as in the oil and gas industry, in the chemical and process industry as well as in the safety analysis of nuclear power plants.

In Norway, the oil and gas industry is of particular importance. Oil and gas fields are often situated far from the shore, and at great depths. This increases the drive towards field developments based on sub-sea processing and multiphase flow transportation. Therefore, it is of significance to be able to predict the flows in greater detail. For this purpose, good and rigorous mathematical models and accurate numerical methods to solve them are required.

The aim of this work is the study of two-phase flows using numerical analysis. In particular, this work presents a five-equation model which will be applied to these particular flows. The results obtained from this model will be used to compare to previous studies based on models with four and six equations [11]. In this context, this thesis can be viewed as a new contribution to these studies carried out by SINTEF.

The Master's Thesis is organized as follows:

Chapter 2 presents the numerical methods we consider in this work. It introduces the *finite folume method* followed by different numerical schemes to determine the intercell flux function. The notion of formally path-consistent schemes is also covered, leading the study of complex nonconservative system of equations.

In Chapter 3, different models of equations of state are introduced.

Chapter 4 is dedicated to the numerical resolution of the Euler equations for a single phase flow. In particular, it shows numerical results for three different types of equations of state. Some of them can be directly compared to previous works [12].

The modelling of a five-equation system to describe two-phase flows is carried

out in Chapter 5. Particularly, the application of the Roe method is explained in detail. Furthermore, comparisons between different numerical schemes as well as between the four-, five- and six-equation models are presented.

Finally, Chapter 6 summarizes all the results obtained in the previous chapters.

Chapter 2

Numerical methods for fluid dynamics

Numerical methods replace the *continuous* problem represented by the PDEs by a *finite* set of *discrete* values by discretising the domain of the PDEs into a finite set of points or volumes via a *mesh* or *grid*.

Different programs can be used in order to solve fluid problems numerically. All the calculations presented in this work utilised FORTRAN 90.

2.1 Quasilinear form

Consider first a system of PDEs of the form

$$U_t + F(U)_x = 0. \tag{2.1}$$

also called a system of *conservation laws*.

Then, the expression

$$U_t + AU_x = 0, \tag{2.2}$$

with

$$A = \frac{\partial F}{\partial U} \tag{2.3}$$

is called the *quasi-linear* form of (2.1). U is the column-vector of *conserved variables* and A is called the Jacobian matrix of the flux function $F(U)$. When considering a *hyperbolic* system of PDEs, the eigenvalues of A represent physically the speeds of propagation of information.

2.2 The Riemann problem

To solve any system of equations presented in the form (2.1) or (2.2) it is necessary to define the Initial Value Problem (IVP) for the conservation laws. The Riemann problem consists on the system (2.1) combined with the initial conditions (IC)

$$U(x,0) = \begin{cases} U_L & x < x_0, \\ U_R & x \geq x_0. \end{cases} \tag{2.4}$$

2.3 Finite volume method

According to Toro [12], computing solutions containing discontinuities, such as shock waves, can present problems depending on the formulation and numerical schemes used. Toro highlights in his book the fact that formulations based on variables other than the conserved variables, fail at shock waves. Therefore, it is recommended to work with conservative methods if shock waves are part of the solution.

The finite volume method regards the discrete values of the domain of (2.1) as *averages over finite volumes*. This method keeps the conservative form of a system of equations. For one spatial dimension, each cell corresponds to a control volume placed around each node of the mesh, as shown in Figure 2.1.

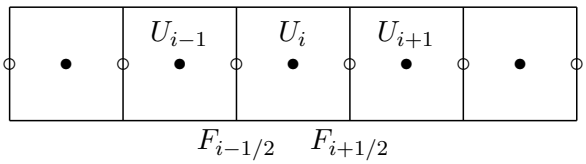

Figure 2.1: The finite volume mesh with a control volume around each node.

Denote de ith grid cell by

$$\mathcal{C}_i = \left(x_{i-1/2}, x_{i+1/2}\right), \tag{2.5}$$

then the value U_i^n will approximate the average value over the ith interval at time t_n

$$U_i^n \approx \frac{1}{\Delta x}\int_{x_{i-1/2}}^{x_{i+1/2}} U\left(x, t_n\right) \mathrm{d}x \equiv \frac{1}{\Delta x}\int_{\mathcal{C}_i} U\left(x, t_n\right) \mathrm{d}x, \tag{2.6}$$

where $\Delta x = x_{i+1/2} - x_{i-1/2}$ is the length of the cell.

The basic *integral form* of a conservation law can be written as

$$\frac{\mathrm{d}}{\mathrm{d}t}\int_{x_1}^{x_2} U\left(x, t\right) \mathrm{d}x = F_1\left(t\right) - F_2\left(t\right) \tag{2.7}$$

where $+F_1\left(t\right)$ and $-F_2\left(t\right)$ represent fluxes *into* the section (intercell fluxes). Using this expression, one can approximate U_i^{n+1}, the cell average at time t_{n+1}, by integrating (2.7) in time from t_n to t_{n+1}

$$\begin{aligned}\frac{1}{\Delta x}\int_{C_i} U\left(x, t_{n+1}\right) \mathrm{d}x =& \frac{1}{\Delta x}\int_{C_i} U\left(x, t_n\right) \mathrm{d}x \\ &- \frac{1}{\Delta x}\left[\int_{t_n}^{t_{n+1}} F\left(U(x_{i+1/2}, t)\right) \mathrm{d}t \right. \\ &\left. - \int_{t_n}^{t_{n+1}} F\left(U(x_{i-1/2}, t)\right) \mathrm{d}t\right].\end{aligned} \tag{2.8}$$

This suggests that one should study numerical methods of the form

$$U_i^{n+1} = U_i^n - \frac{\Delta t}{\Delta x}\left(F_{i+1/2}^n - F_{i-1/2}^n\right), \tag{2.9}$$

where $F_{i-1/2}^n$ is some approximation to the average flux along $x = x_{i-1/2}$. This expression can be made accurate to arbitrary order: F can be a function of higher

orders in Δt and Δx. Moreover, Runge-Kutta methods can be employed to obtain higher order in time.

The challenge in the finite volume methods is to find an accurate and computationally inexpensive approximation to the intercell flux.

2.4 The Lax-Friedrichs scheme

It is one of the most simple and robust schemes for the intercell flux. This flux is given by

$$F^n_{i-1/2} = \frac{1}{2}\left(F^n_{i-1} + F^n_i\right) - \frac{1}{2}\frac{\Delta x}{\Delta t}\left(U^n_i - U^n_{i-1}\right). \tag{2.10}$$

This method is stable for a hyperbolic system if $\Delta x/\Delta t \geq |\lambda^m|$, where $|\lambda^m|$ is the largest eigenvalue of the Jacobian matrix (2.3). This is called the *CFL condition* and the number $|\lambda^m| \cdot \Delta t/\Delta x$ is called the *CFL number*.

2.5 The Riemann solver of Roe

The Roe method approximates a non-linear system of equations written in the form (2.1) combined with the Riemann problem (2.4) by replacing the Jacobian matrix with a *constant* matrix locally linearised. Following the nomenclature utilised by LeVeque [6] and Munkejord [8], this can be written as

$$\hat{A}_{i-1/2} = \hat{A}_{i-1/2}\left(U_{i-1}, U_i\right), \tag{2.11}$$

where $\hat{A}_{i-1/2}$ is a function of the neighbourhood data U_{i-1}, U_i.

Therefore, the original Riemann problem (2.4) is replaced by a *linear approximate Riemann problem* defined locally at each cell interface

$$\begin{cases} U_t + \hat{A}_{i-1/2} U_x = 0, \\ U\left(x, 0\right) = \begin{cases} U_L & x < x_0, \\ U_R & x \geq x_0. \end{cases} \end{cases} \tag{2.12}$$

The matrix $\hat{A}_{i-1/2}$ is called the Roe matrix and has the following properties, also known as the Roe conditions:

1. $\hat{A}_{i-1/2}$ must retain the hyperbolicity of the system. The Roe matrix is diagonalizable with real eigenvalues.

2. It must be consistent with the exact Jacobian, that is $\hat{A}_{i-1/2}\left(U, U\right) = A\left(U\right)$.

3. It is conservative across discontinuities: $\hat{A}_{i-1/2}\left(U_i - U_{i-1}\right) = F\left(U_i\right) - F\left(U_{i-1}\right)$.

The latter condition is derived from imposing the property on $\hat{A}_{i-1/2}$ that if U_{i-1} and U_i are connected by a single wave $\mathcal{W}^p = U_i - U_{i-1}$ in the Riemann solution, then $\mathcal{W}^p$ should also be an eigenvector of $\hat{A}_{i-1/2}$.

The Roe matrix can also be expressed as

$$|\hat{A}_{i-1/2}| = \hat{R}_{i-1/2} |\hat{\Lambda}_{i-1/2}| \hat{R}^{-1}_{i-1/2}, \tag{2.13}$$

where $\hat{R}_{i-1/2}$ is the matrix having the right eigenvectors $\hat{r}_{i-1/2}$ of $\hat{A}_{i-1/2}$ as its columns, and $|\hat{\Lambda}_{i-1/2}|$ is the diagonal matrix containing the absolute value of the eigenvalues $|\hat{\lambda}_{i-1/2}|$ of $\hat{A}_{i-1/2}$.

The approximate Riemann solution consists of m waves proportional to the eigenvectors $\hat{r}_{i-1/2}$ of $\hat{A}_{i-1/2}$, propagating with speeds

$$s^p_{i-1/2} = \hat{\lambda}^p_{i-1/2} \tag{2.14}$$

given by the eigenvalues. These waves can be found through the proportionality coefficients $\beta^p_{i-1/2}$ by solving the linear system

$$U_i - U_{i-1} = \sum_{p=1}^{m} \beta^p_{i-1/2} \hat{r}^p_{i-1/2}. \tag{2.15}$$

These coefficients can be interpreted as wave strengths. The solution of the previous equation is

$$\beta^p_{i-1/2} = \hat{R}^{-1}_{i-1/2} \left(U_i - U_{i-1}\right), \tag{2.16}$$

where the waves can be found as

$$\mathcal{W}^p_{i-1/2} = \beta^p_{i-1/2} \hat{r}^p_{i-1/2}, \tag{2.17}$$

Finally, an expression for the inter-cell flux may be written as

$$F_{i-1/2} = \frac{1}{2}\Big(F\left(U_{i-1}\right) + F\left(U_i\right)\Big) - \frac{1}{2}|\hat{A}_{i-1/2}|\left(U_i - U_{i-1}\right). \tag{2.18}$$

The remaining difficulty of the Roe method is actually finding the Roe matrix $\hat{A}_{i-1/2}$.

2.5.1 Linearization strategies

In the event that the flux F is a rational function of the components of U, Roe discusses two strategies to find $\hat{A}_{i-1/2}$.

Direct algebraic manipulation

Consider the discrete variants of the differential rules for rational functions:

$$\Delta\left(p \pm q\right) = \Delta p \pm \Delta q, \tag{2.19}$$

$$\Delta\left(pq\right) = \bar{p}\Delta q + \bar{q}\Delta p, \tag{2.20}$$

$$\Delta\left(1/q\right) = -\Delta q/\tilde{q}^2, \tag{2.21}$$

where $\bar{(\cdot)}$ denotes an arithmetic and $\tilde{(\cdot)}$ denotes a geometric mean value. For any rational function $y\left(x_1, \ldots, x_n\right)$, any jump Δy can generally be written in terms of jumps in x_r as

$$\Delta y\left(x_1, \ldots, x_n\right) = \sum_{r=1}^{n} k_r \Delta x_r, \tag{2.22}$$

where the coefficients k_r are obtained by repeated application of (2.19)-(2.21) to Δy.

Then (2.22) may be extended to the flux vector $F(U)$ to yield

$$f_m(U^R) - f_m(U^L) = \sum_n \hat{a}_{mn} \left(u_n^R - u_n^L \right), \tag{2.23}$$

where $\hat{a}_{mn}$, constructed by repeated application of (2.19)-(2.21), are the entries of $\hat{A}_{i-1/2}$. Here, $(\cdot^L) = (\cdot_{i-1})$ and $(\cdot^R) = (\cdot_i)$ represent the left side and the right side terms of the Roe average.

Parameter vectors

Assume that F and U may be expressed through a change of variables as

$$F = F(\chi), \tag{2.24}$$
$$U = U(\chi), \tag{2.25}$$

for some parameter vector $\chi(U)$, where the components of F are at most quadratic polynomials in the components of χ. Then, by (2.19) and (2.20), any jump in F is related to jumps in χ exclusively through *arithmetic* averages, and the Roe matrix may be obtained as

$$\hat{A}(U^R, U^L) = A\left(U((\chi^L + \chi^R)/2) \right). \tag{2.26}$$

2.5.2 High-resolution terms

A high-resolution extension for the Roe method is described by LeVeque [6] as

$$U_i^{n+1} = U_i^n - \frac{\Delta t}{\Delta x} \left(\mathcal{A}^- \Delta U_{i+1/2} + \mathcal{A}^+ \Delta U_{i-1/2} \right) - \frac{\Delta t}{\Delta x} \left(\hat{F}_{i+1/2} - \hat{F}_{i-1/2} \right). \tag{2.27}$$

The waves and wave speeds from the approximate Riemann solution are used to define

$$\mathcal{A}^- \Delta U_{i-1/2} = \sum_{p=1}^{m} \left(s_{i-1/2}^p \right)^- \mathcal{W}_{i-1/2}^p, \tag{2.28}$$

$$\mathcal{A}^+ \Delta U_{i-1/2} = \sum_{p=1}^{m} \left(s_{i-1/2}^p \right)^+ \mathcal{W}_{i-1/2}^p, \tag{2.29}$$

where $\mathcal{W}_{i-1/2}^p$ is the pth wave arising in the solution to the Riemann problem at $x_{i-1/2}$. m is the number of waves and, since a linearised Riemann solver is used, it is equal to the number of equations. $s_{i-1/2}^p$ is the wave speed of the pth wave and can also be expressed as

$$\left(s_{i-1/2}^p \right)^\pm = \frac{1}{2} \left(s_{i-1/2}^p \pm |s_{i-1/2}^p| \right). \tag{2.30}$$

The flux vector $\hat{F}_{i-1/2}$ is what LeVeque calls the high-resolution correction given by

$$\hat{F}_{i-1/2} = \frac{1}{2} \sum_{p=1}^{m} |s_{i-1/2}^p| \left(1 - \frac{\Delta t}{\Delta x} |s_{i-1/2}^p| \right) \widehat{\mathcal{W}}_{i-1/2}^p, \tag{2.31}$$

where $\widehat{\mathcal{W}}^p$ is a limited version of the wave $\mathcal{W}^p_{i-1/2}$.

The limited waves are found by comparing the wave $\mathcal{W}^p_{i-1/2}$ with the upwind wave $\mathcal{W}^p_{I-1/2}$ where

$$I = \begin{cases} i-1 & s^p_{i-1/2} \geq 0, \\ i+1 & s^p_{i-1/2} < 0. \end{cases} \tag{2.32}$$

The relation between these two waves is given by

$$\widehat{\mathcal{W}}^p_{i-1/2} = \phi(\theta^p_{i-1/2})\mathcal{W}^p_{i-1/2}, \tag{2.33}$$

where ϕ is the flux-limiter function, and $\theta^p_{i-1/2}$ is a measure of the smoothness of the pth characteristic component of the solution:

$$\theta^p_{i-1/2} = \frac{\mathcal{W}^p_{I-1/2} \cdot \mathcal{W}^p_{i-1/2}}{\mathcal{W}^p_{i-1/2} \cdot \mathcal{W}^p_{i-1/2}}. \tag{2.34}$$

Herein $\cdot$ denotes the scalar product in $\mathbb{R}^m$.

High-resolution limiters

The high-resolution limiters produce methods that are formally first-order, but they approach second-order methods for smooth solutions.

One of these limiters is the Monotonized Central difference (MC), which is defined by

$$\phi(\theta) = \max(0, \min((1+\theta)/2, 2, 2\theta)). \tag{2.35}$$

2.5.3 Harten's entropy fix

According to Toro [12], linearised Riemann problem solutions (given in this case, by the Roe method) consist of discontinuous jumps only, which means that they can provide a good approximation for contacts and shocks. Rarefaction waves, on the other hand, consist of a continuous change in the flow variables. As time increases, they tend to spread and the linearised approximation by discontinuous jumps becomes grossly incorrect. In a numeric context, only when the rarefaction is *transonic* or *sonic*, the linearised approximations encounter difficulties giving unphysical results in the form of entropy violating discontinuous waves.

Another possibility of viewing the effect of the entropy violation is commented by LeVeque [6]. The second term in the right-side of the Roe flux relation (2.18), also called the viscous term, will be close to zero in a transonic rarefaction, as the eigenvalues related to the sound speed could tend to zero. With sufficient viscosity, one should not observe entropy-violating shocks.

Harten's entropy fix is based on increasing the viscosity by modifying $|\hat{\lambda}_{i-1/2}|$ appearing in (2.13), never allowing any eigenvalue $\hat{\lambda}_{i-1/2}$ to be too close to zero

$$\phi_\delta(\hat{\lambda}_j) = \begin{cases} |\hat{\lambda}_j| & |\hat{\lambda}_j| \geq \delta, \\ (\hat{\lambda}_j^2 + \delta^2)/2\delta & |\hat{\lambda}_j| < \delta. \end{cases} \tag{2.36}$$

A disadvantage of this approach is that the parameter δ must be typically tuned to the problem.

When the high-resolution extension for the Roe method is used, the Harten's entropy fix is achieved by redefining the relation (2.30) employed for the wave speed in the equation (2.27)

$$\lambda^{\pm} = \frac{1}{2}\left(\lambda \pm \ \phi_{\delta}(\lambda)\right). \tag{2.37}$$

2.6 The Rough scheme

The Rough scheme consists on imposing a Roe-like flux of the form

$$F_{i-1/2} = \frac{1}{2}\Big(F\left(U_{i-1}\right) + F\left(U_i\right)\Big) - \frac{1}{2}|\bar{A}_{i-1/2}|\left(U_i - U_{i-1}\right), \tag{2.38}$$

where, for example, one can choose $\bar{A}_{i-1/2} = A\left(\left(U_{i-1} + U_i\right)/2\right)$, A being the Jacobian matrix of the system. The matrix $|\bar{A}_{i-1/2}|$ can also be decomposed as

$$|\bar{A}_{i-1/2}| = \bar{R}_{i-1/2}|\bar{\Lambda}_{i-1/2}|\bar{R}^{-1}_{i-1/2}, \tag{2.39}$$

as reported previously for the Roe method.

2.7 Numerical formally path-consistent schemes

According to [11], the class of numerical *conservative* schemes for conservation laws like those presented above, are a special case of the more general class of *formally path-consistent* schemes.

Given a *nonconservative* system of balance laws of the form

$$U_t + F\left(U\right)_x + B\left(U\right)W\left(U\right)_x = S\left(U\right), \tag{2.40}$$

a scheme in the form

$$\frac{U_i^{n+1} - U_i^n}{\Delta t} + \frac{F_{i+1/2} - F_{i-1/2}}{\Delta x} + \frac{D^+_{i-1/2} + D^-_{i+1/2}}{\Delta x} = S_i, \tag{2.41}$$

where

$$D^+_{i+1/2} = B_{i+1/2}\left(W_{i+1} - W_{i+1/2}\right), \tag{2.42}$$

$$D^-_{i+1/2} = B_{i+1/2}\left(W_{i+1/2} - W_i\right), \tag{2.43}$$

$$B_{i+1/2} = \frac{B_i + B_{i+1}}{2} \tag{2.44}$$

is formally consistent with a certain family of paths (an exhaustive demonstration of this statement can be found at [11]). These new nonconservative schemes will satisfy the following properties:

1. The schemes should reduce to their standard conservative formulation if the matrix B is constant:

   $$\frac{\partial U}{\partial t} + \frac{\partial G\left(U\right)}{\partial x} = 0, \tag{2.45}$$

   with

   $$G \equiv F + BW \tag{2.46}$$

   whenever B is constant.

2. The schemes should be formally path-consistent.

Chapter 3

Thermodynamic considerations

A system of PDEs such as (2.1) to solve fluid problems is insufficient to fully describe the physical processes involved. There are more unknowns than equations and thus closure conditions are required. This can be solved by introducing an *equation of state* (EOS).

In the $p-v-T$ systems, defined by the pressure, specific volume and temperature, one can relate these variables via the *thermal equation of state*. This chapter presents different EOSes which will be applied in the numerical resolution of fluid problems.

3.1 Isothermal gas

The EOS for this special case is

$$p = p(\rho) \equiv \rho c^2, \tag{3.1}$$

where ρ is the density of the fluid and c is a non-zero *constant* propagation speed of sound.

3.2 Isentropic gas

This EOS is given by

$$p = p(\rho) \equiv C\rho^\gamma, \quad C \equiv \text{constant}, \tag{3.2}$$

where γ is the *ratio of specific heats* or *adiabatic exponent* defined as

$$\gamma = \frac{c_p}{c_v}, \tag{3.3}$$

where c_p and c_v are the specific heat capacities at a constant pressure and volume, respectively.

3.3 Ideal gas

The ideal thermal EOS can be expressed as

$$pV = n\mathcal{R}T, \tag{3.4}$$

where V is the volume, $\mathcal{R} = 8.134\,\mathrm{J\,mol^{-1}\,K^{-1}}$ is the Universal Gas Constant, and T is the absolute temperature.

3.4 Stiffened gas equation of state

This EOS can be written as a pressure law

$$p(\rho, e) = (\gamma - 1)\,\rho\,(e - e_*) - \gamma p_\infty, \tag{3.5}$$

where e is the internal energy of the fluid; γ, e_* and p_∞ are constants specific to the fluid. Herein, e_* becomes relevant when phase transitions are involved: not taken into account in this work. On the other hand, p_∞ leads to the *stiffened* properties compared to ideal gases (note in particular that $p_\infty = 0$ leads to the ideal-gas law).

The sound velocity is given by the expression

$$c = \sqrt{\left(\frac{\partial p}{\partial \rho}\right)_s} = \sqrt{\gamma \frac{p + p_\infty}{\rho}}, \tag{3.6}$$

where p_∞ can be interpreted as a parameter that *stiffens* an ideal gas by increasing its sound velocity.

According to the common literature [3], the density can be expressed as

$$\rho = \frac{p + p_\infty}{(\gamma - 1)\,c_v T}. \tag{3.7}$$

The internal energy is given by

$$e = \frac{c_p}{\gamma} T + \frac{p_\infty}{\rho} + e_*. \tag{3.8}$$

The entropy can be written as

$$s = c_v \ln\left(\frac{p + p_\infty}{\rho^\gamma}\right). \tag{3.9}$$

Chapter 4

Numerical resolution of the Euler equations

This chapter introduces, as a preliminary study of the more complex multiphase flows, the one-dimensional Euler equations. The aim of this chapter is to show the numerical methods applied to this particular system of equations in order to be able to understand the numerical treatment of multiphase flows.

4.1 The conservation-law form of the Euler equations

The one-dimensional Euler equations is a system of non-linear hyperbolic equations that governs the dynamics of a compressible fluid for which the effects of body forces, viscous stresses and heat flux are neglected.

In vector notation this system reads

$$U_t + F(U)_x = \mathbf{0}, \tag{4.1}$$

with

$$U = \begin{bmatrix} \rho \\ \rho v \\ E \end{bmatrix}, \quad F(U) = \begin{bmatrix} \rho v \\ \rho v^2 + p \\ v(E+p) \end{bmatrix}. \tag{4.2}$$

The variables ρ, v, p and E are the density, velocity, pressure and total energy of the fluid, respectively. U is the column vector of conserved variables and $F(U)$ is the flux vector in the x direction. As discussed in Section 2.1, the system (4.1) represents a system of conservation laws.

4.2 Quasilinear form

The system (4.1) can also be written in quasilinear form

$$U_t + AU_x = 0, \tag{4.3}$$

with

$$A(U) = \frac{\partial F}{\partial U} = \begin{bmatrix} \partial f_1/\partial u_1 & \partial f_1/\partial u_2 & \partial f_1/\partial u_3 \\ \partial f_2/\partial u_1 & \partial f_2/\partial u_2 & \partial f_2/\partial u_3 \\ \partial f_3/\partial u_1 & \partial f_3/\partial u_2 & \partial f_3/\partial u_3 \end{bmatrix}. \tag{4.4}$$

In this hyperbolic system, the eigenvalues of the Jacobian matrix are

$$\lambda_1 = v - c, \quad \lambda_2 = v, \quad \lambda_3 = v + c, \tag{4.5}$$

where c is the speed of sound. The eigenvectors associated to these eigenvalues are

$$K_1 = \begin{bmatrix} 1 \\ v - c \\ H - vc \end{bmatrix}, \quad K_2 = \begin{bmatrix} 1 \\ v \\ v^2/2 \end{bmatrix}, \quad K_3 = \begin{bmatrix} 1 \\ v + c \\ H + vc \end{bmatrix}, \tag{4.6}$$

where H is the total enthalpy

$$H = \frac{E + p}{\rho}. \tag{4.7}$$

4.3 Closure considerations

In order to solve the problem (4.1), one must add an EOS. From now on, only isothermal, isentropic and ideal EOSes are going to be considered.

For the isothermal and isentropic EOSes the pressure is related, in a direct way, to another variable such as the density or a constant, as one can see in (3.1) and (3.2) respectively, closing easily the problem.

When the ideal gas EOS is considered, this relation is less straightforward. One way of combining the system (4.1) with the ideal thermal EOS (3.4) is by using the expression of the total energy

$$E = \rho e + \frac{1}{2}\rho v^2, \tag{4.8}$$

In the particular case of an ideal gas, e is only a function of the temperature

$$e = c_v T, \tag{4.9}$$

and it is possible to relate c_v and $\mathcal{R}$ through the relation

$$c_v = \frac{\mathcal{R}}{\gamma - 1}, \tag{4.10}$$

and consequently arrive to a new expression for the total energy

$$E = \frac{1}{2}\rho v^2 + \frac{p}{(\gamma - 1)\,\rho}, \tag{4.11}$$

closing finally the problem.

Once the problem is closed, it is possible to apply one of the numerical schemes already discussed.

4.4 Numerical tests

This section presents the numerical results obtained by resolving the Riemann problem (2.4) applied to the system (4.1) using three different EOSes and the Lax-Friedrichs and Roe schemes for the intercell flux.

4.4.1 Isothermal gas

Numerical simulations were performed on a grid representing the unit interval with up to 1000 cells. The initial conditions were zero velocity and a density discontinuity: $\rho_L = 1.4$ and $\rho_R = 1$ at $x = 0.5$. The speed of sound was $c = 1$ and therefore the values of the pressure were fixed. The simulation time was up to 0.35 units using a CFL number 0.5. The solution of this problem consists on two density and velocity waves propagating away from the initial discontinuity.

Figure 4.1 shows the density profiles at $t = 0.35$ for different number of cells using the Lax-Friedrichs scheme, Figure 4.1(a), and the Roe scheme, Figure 4.1(b). In both cases, it is possible to appreciate that the results converge as the number of cells increases. It is important to note that, for the same number of cells, the Lax-Friedrichs scheme smears the solution more than the Roe method.

Figure 4.2 shows the velocity profiles, Figure 4.2(a), and the pressure profiles, Figure 4.2(b), at different times. They have been obtained using the Roe method on a grid of 500 cells.

4.4.2 Isentropic gas

Numerical simulations were performed using the same procedure as in the previous section. Nevertheless, the isentropic gas EOS requires the definition of the constant C in equation (3.2) instead of using a constant value for the sound speed. The value $\gamma = 1.4$ was chosen during the simulations. The initial conditions were zero velocity and a discontinuity at $x = 0.5$ in the density, $\rho_L = 1.4$ and $\rho_R = 1$, and in the pressure. For the left-hand side of the discontinuity $p_L = 1.4$ was chosen and then, the value of C was calculated using (3.2). The value $p_R \approx 0.89$ was determined using once more (3.2). The simulation time was up to 0.35 units using a CFL number 0.5. The nature of the solution of this problem is similar to that of the isothermal gas.

Figure 4.3 shows the density profiles at $t = 0.35$ for different number of cells using the Lax-Friedrichs scheme, Figure 4.3(a), and the Roe scheme, Figure 4.3(b). The same conclusions as in the isothermal gas can be applied to the isentropic gas.

Figure 4.4 shows the velocity profiles, Figure 4.4(a), and the pressure profiles, Figure 4.4(b), at different times. They have been obtained using the Roe method on a grid of 500 cells, as in the isothermal case. Note the difference between Figures 4.2(b)-4.4(b) in the values at the boundaries.

4.4.3 Ideal gas

The simulations performed in this case were inspired by a *modified version* of the popular Sod's test extracted from Section 11.5.1 of the book of Toro [12]. It consists on a discontinuity at $x = 0.3$ in a unit-interval grid with the following values for the primitive variables: $\rho_L = 1$, $u_L = 0.75$, $p_L = 1$; $\rho_R = 0.125$, $u_R = 0$ and $p_R = 0.1$. The solution to this test consists of a right shock wave, a right-travelling contact wave and a left *sonic* rarefaction wave, so that the entropy fix will be necessary when the Roe scheme will be utilised.

As in the previous case, $\gamma = 1.4$ was adopted. The simulation time was 0.2 units using a CFL number 0.9 and up to 2000 grid cells. These values are the same as

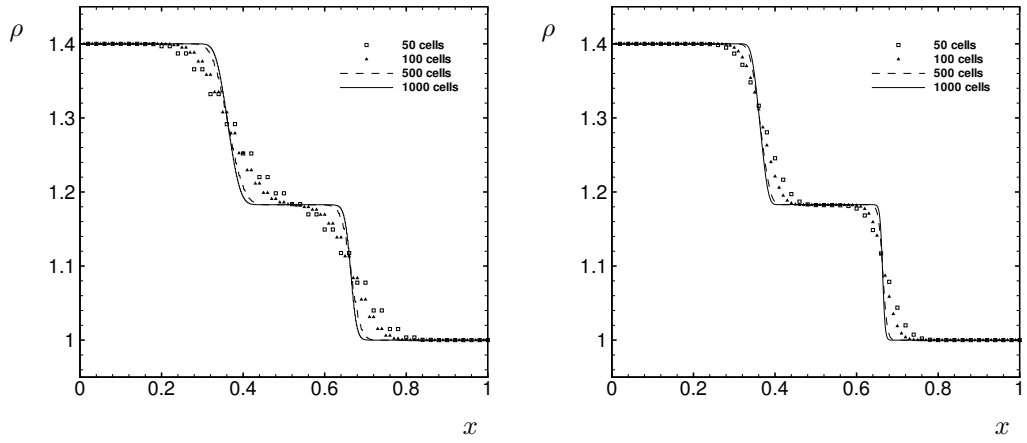

(a) Lax-Friedrichs scheme. (b) Roe scheme.

Figure 4.1: Isothermal gas. Riemann problem with a discontinuity in the density at $x = 0.5$. Convergence of the density profiles using the Lax-Friedrichs scheme (a) and the Roe scheme (b). The CFL number was 0.5.

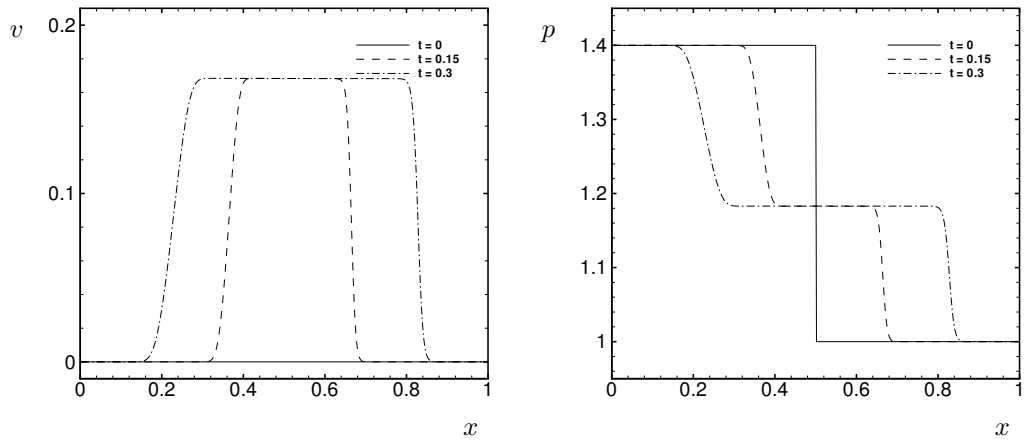

(a) Velocity profiles. (b) Pressure profiles.

Figure 4.2: Isothermal gas. Riemann problem with a discontinuity in the density at $x = 0.5$ solved using the Roe scheme on a grid of 500 cells. Results for the velocity profile (a) and for the pressure profile (b) for three different times. The CFL number was 0.5.

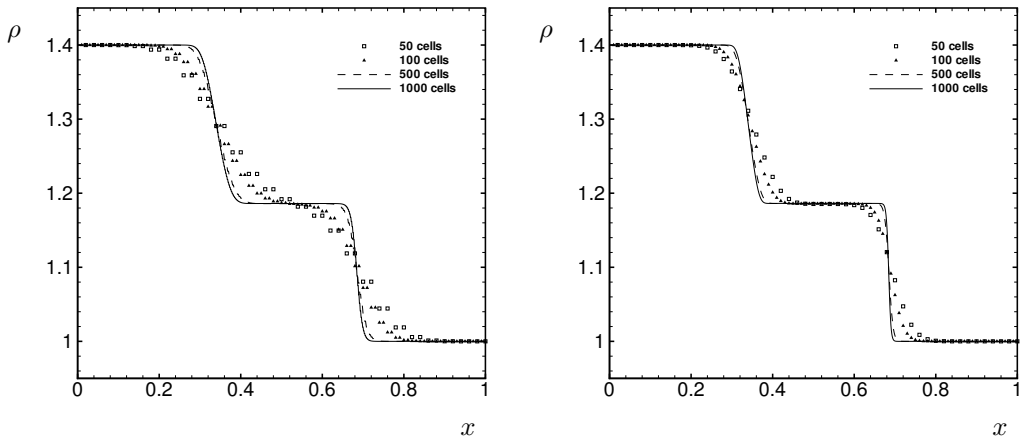

(a) Lax-Friedrichs scheme. (b) Roe scheme.

Figure 4.3: Isentropic gas. Riemann problem with a discontinuity at $x = 0.5$. Convergence of the density profiles using the Lax-Friedrichs scheme (a) and the Roe scheme (b). The CFL number was 0.5.

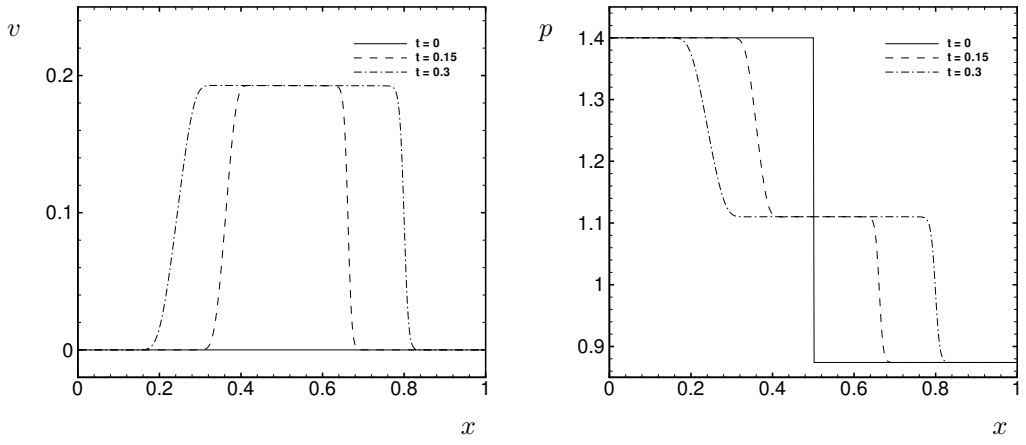

(a) Velocity profiles. (b) Pressure profiles.

Figure 4.4: Isentropic gas. Riemann problem with a discontinuity at $x = 0.5$ solved using the Roe scheme on a grid of 500 cells. Results for the velocity profile (a) and for the pressure profile (b) for three different times. The CFL number was 0.5.

those utilised by Toro so that the results obtained can be directly compared to those illustrated in Figure 11.5 of his book.

Figure 4.5 shows the density, velocity, pressure and internal energy profiles at $t = 0.2$ for a grid composed of 100 cells using the Roe method with and without the Harten's entropy fix. The results are compared with those obtained using 2000 grid cells. As a matter of fact, near the sonic point, the Roe scheme together with the entropy fix provide a physically valid solution.

In order to compare the solutions obtained with the Lax-Friedrichs and the Roe methods, Figure 4.6 shows how the Lax-Friedrichs scheme is more diffusive than the Roe scheme, for the same number of cells. Since the Lax-Friedrichs scheme does not resolve a linear approximated Riemann problem, the entropy violation is not observed when this scheme is used.

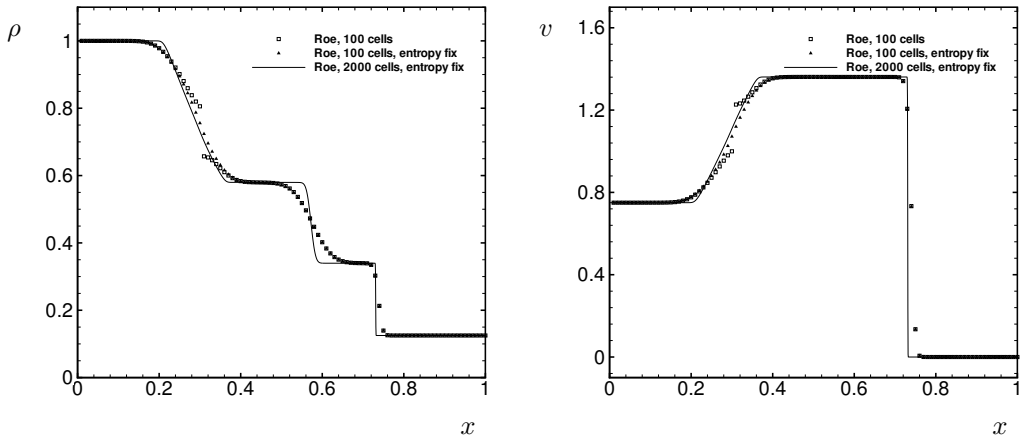

(a) Density. (b) Velocity.

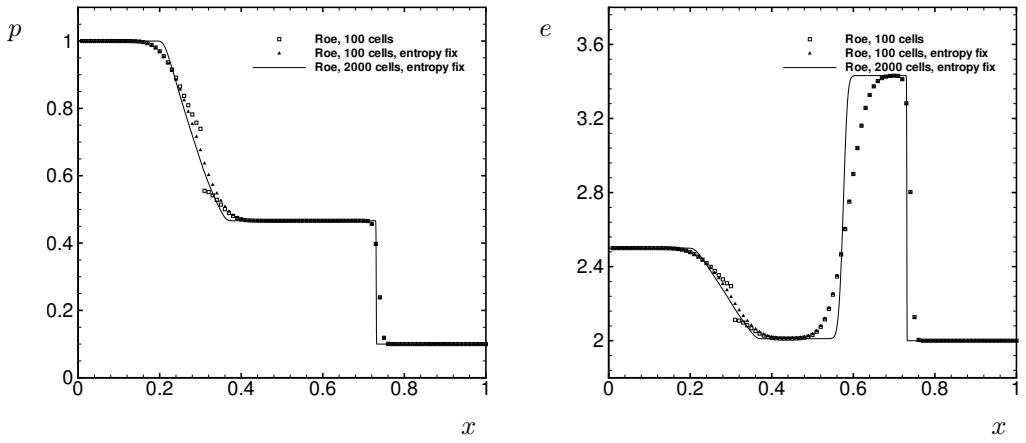

(c) Pressure. (d) Internal energy.

Figure 4.5: Ideal gas. Riemann problem with a discontinuity at $x = 0.3$. Density (a), velocity (b), pressure (c) and internal energy (d) profiles solved using the Roe method with and without the Harten's entropy fix. The CFL number was 0.9.

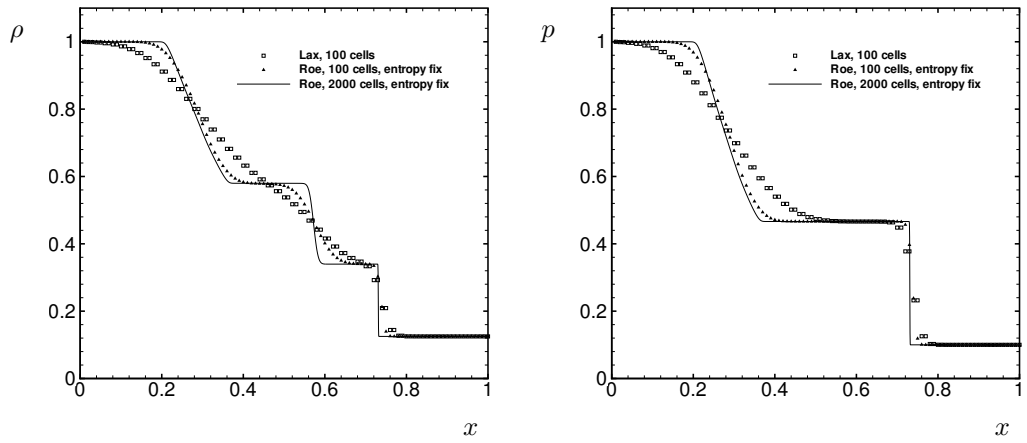

(a) Density. (b) Pressure.

Figure 4.6: Ideal gas. Riemann problem with a discontinuity at $x = 0.3$. Density (a) and pressure (b) profiles solved using the Lax-Friedrichs and Roe schemes. The CFL number was 0.9.

Chapter 5

Numerical resolution of a five-equation model

This chapter presents the numerical resolution of a simultaneous flow of two fluids through a transport pipeline. The five-equation model introduces the equality of temperatures of the flows as a simplification. This is a relatively valid approximation in pipelines, where the temperatures of the flows are not too different.

Furthermore, this five-equation model presents certain complexity compared to other models such as the four-equation model in which the temperatures of the fluids are not taken into account. More complex models like the six-equation model present an energy equation to each phase and, therefore, the study of heat transfers between the phases must be considered. In this context, the five-equation model can be a good approximation whenever the difference of temperatures of the phases does not become important.

5.1 The two-phase five-equation flow model

The classical two-fluid model is based on balance laws for mass, momentum and energy for each phase: gas and liquid. In this work, the viscous terms are neglected and each phase is equipped with an equation of state written in the form

$$p_k = p_k\left(\rho_k, e_k\right), \tag{5.1}$$

for $k \in \{g, l\}$. As a simplification, *mechanical equilibrium* and *thermal equilibrium* between the phases are assumed

$$p = p_g\left(\rho_g, e_g\right) = p_l\left(\rho_l, e_l\right), \tag{5.2}$$

$$T = T_g = T_l. \tag{5.3}$$

If no mass transfer is assumed between the phases and all external forces but gravity are ignored, one can obtain a system of equations in which the mass and

momentum equations may be written as follows

$$\frac{\partial \rho_g \alpha_g}{\partial t} + \frac{\partial \rho_g \alpha_g v_g}{\partial x} = 0, \tag{5.4}$$

$$\frac{\partial \rho_l \alpha_l}{\partial t} + \frac{\partial \rho_l \alpha_l v_l}{\partial x} = 0, \tag{5.5}$$

$$\frac{\partial \rho_g \alpha_g v_g}{\partial t} + \frac{\partial \rho_g \alpha_g v_g^2}{\partial x} + \alpha_g \frac{\partial p}{\partial x} + \tau_i = \rho_g \alpha_g g_x, \tag{5.6}$$

$$\frac{\partial \rho_l \alpha_l v_l}{\partial t} + \frac{\partial \rho_l \alpha_l v_l^2}{\partial x} + \alpha_l \frac{\partial p}{\partial x} - \tau_i = \rho_l \alpha_l g_x, \tag{5.7}$$

where ρ_k, α_k, and v_k represent the density, volume fraction and velocity of each phase, respectively. In addition, g_x represents the gravity along the x-axis and the term τ_i is the interface momentum-exchange.

Note that these two phases are sharing a common volume V. The volume fraction of the phase k is therefore defined by

$$\alpha_k = \frac{V_k}{V}, \tag{5.8}$$

where V_k is the total volume occupied by this phase, given by

$$V_k = \frac{M_k}{\rho_k}, \tag{5.9}$$

where M_k is the total mass of the phase k in the volume V.

Consistency requires then that the sum of the volume fractions of all the present phases equals Unity

$$\sum_k \alpha_k = 1. \tag{5.10}$$

Additionally, it is possible to deduce an expression for the *total energy* of the system by summing the energy-balance equations of each phase

$$\frac{\partial E_g}{\partial t} + \frac{\partial}{\partial x}\Big(E_g v_g + \alpha_g v_g p\Big) + p\frac{\partial \alpha_g}{\partial t} = \rho_g \alpha_g v_g g_x, \tag{5.11}$$

$$\frac{\partial E_l}{\partial t} + \frac{\partial}{\partial x}\Big(E_l v_l + \alpha_l v_l p\Big) + p\frac{\partial \alpha_l}{\partial t} = \rho_l \alpha_l v_l g_x. \tag{5.12}$$

where

$$E_k = \rho_k \alpha_k \left(e_k + \frac{1}{2} v_k^2\right) \tag{5.13}$$

is the *total phasic energy* obtained as the sum of the internal energy e_k and the kinetic energy. The total energy can then be expressed as

$$\frac{\partial E}{\partial t} + \frac{\partial}{\partial x}\Big\{E_g v_g + E_l v_l + p\left(\alpha_g v_g + \alpha_l v_l\right)\Big\} = \left(\rho_g \alpha_g v_g + \rho_l \alpha_l v_l\right) g_x, \tag{5.14}$$

It is important to clarify that the system of equations defined by (5.4)-(5.7) and (5.14), also called the *five-equation model*, is a simplification of the *six-equation model*, defined by (5.4)-(5.12), which presents one energy-balance equation for each phase. A *four-equation model* can also be obtained from equations (5.4)-(5.7): note that this model lacks any energy equation.

To get these models a well-defined mathematical solution, a common approach consists on including differential terms in the modelling of τ_i in order to render the system hyperbolic with real eigenvalues

$$\tau_i = \tau_D + \tau_F, \tag{5.15}$$

where τ_D represents added differential terms and τ_F must satisfy entropy conditions: $\tau_F = 0$ will be chosen in this work. In this context, τ_D can be interpreted as a pressure jump δp at the gas-liquid interface

$$\tau_D = -\delta p \frac{\partial \alpha_l}{\partial x}. \tag{5.16}$$

Following [2], δp is given by

$$\delta p = \sigma \frac{\rho_g \alpha_g \rho_l \alpha_l}{\rho_g \alpha_l + \rho_l \alpha_g} \left(v_g - v_l\right)^2, \tag{5.17}$$

where a sufficently large value of σ ensures the hyperbolicity of the system.

5.2 Canonical nonconservative form

Equations (5.4)-(5.7) and (5.14) can be written as a system of hyperbolic partial differential equations in the non-conservative form

$$\frac{\partial U}{\partial t} + \frac{\partial F\left(U\right)}{\partial x} + B\left(U\right) \frac{\partial W\left(U\right)}{\partial x} = S\left(U\right) \tag{5.18}$$

with

$$U = \begin{bmatrix} \rho_g \alpha_g \\ \rho_l \alpha_l \\ \rho_g \alpha_g v_g \\ \rho_l \alpha_l v_l \\ E \end{bmatrix}, \quad F\left(U\right) = \begin{bmatrix} \rho_g \alpha_g v_g \\ \rho_l \alpha_l v_l \\ \rho_g \alpha_g v_g^2 + \alpha_g \delta p \\ \rho_l \alpha_l v_l^2 + \alpha_l \delta p \\ E_g v_g + E_l v_l + p\left(\alpha_g v_g + \alpha_l v_l\right) \end{bmatrix},$$

$$B\left(U\right) = \begin{bmatrix} 0 & 0 \\ 0 & 0 \\ \alpha_g & -\alpha_g \\ \alpha_l & -\alpha_l \\ 0 & 0 \end{bmatrix}, \quad W\left(U\right) = \begin{bmatrix} p \\ \delta p \end{bmatrix}, \tag{5.19}$$

$$S\left(U\right) = \begin{bmatrix} 0 \\ 0 \\ \rho_g \alpha_g g_x \\ \rho_l \alpha_l g_x \\ \left(\rho_g \alpha_g v_g + \rho_l \alpha_l v_l\right) g_x \end{bmatrix}.$$

As it is possible to appreciate, (5.18) is a system of conservation laws augmented with non-conservative products and source terms and, consequently, further complications may arise. A generalization of the classic concept of conservative numerical schemes must be used leading to *path-conservative schemes* (see section 2.7).

5.3 Thermodynamic considerations

In the context of a two-phase fluid model, an EOS has to be applied to each phase $k \in \{g, l\}$ in order to close the system (5.18).

The numerical simulations that will be presented at the end of this chapter will only use the stiffened gas EOS for both phases. Moreover, *mechanical* and *thermal equilibrium* are going to be considered: the pressure and the temperature of both phases will be equal.

5.3.1 Numerical algorithm for the pressure

Assuming always mechanical and thermal equilibrium between the phases and knowing their properties, the problem of associating the system (5.18) with the stiffened gas EOS can be presented as follows (see [3]):

> Given the partial densities $\rho_k \alpha_k$ and the internal energy of the mixture $\sum \rho_k \alpha_k e_k$, calculate the common temperature T, the densities ρ_k, the volume fractions α_k and the common pressure p.

The proposed task can be easily performed if the values of the pressure and the temperature are already given. In fact, once these values are known, one can calculate the densities and the internal energies using the expressions written in Section 3.4.

For this particular EOS, the temperature can be expressed as a function of the pressure

$$T = \frac{\sum \rho_k \alpha_k e_k + p - \sum \rho_k \alpha_k e_{*_k}}{\sum \rho_k \alpha_k c_{p_k}}, \tag{5.20}$$

but the pressure has to be calculated using an iterative process with an algorithm based on the standard Newton-Rapshon method, as described in [3]. According to this paper, the method

$$\hat{p}_{n+1} = \hat{p}_n + \frac{1 - g(\hat{p}_n)}{g'(\hat{p}_n)} \left(1 - \frac{1 - g(\hat{p}_n) + |1 - g(\hat{p}_n)|}{2g'(\hat{p}_n)} h(\hat{p}_n)\right)^{-1}, \tag{5.21}$$

where

$$g(p) = \sum A_k \frac{z}{z + q_k}, \quad g'(p) = \sum A_k \frac{q_k}{(z + q_k)^2}, \tag{5.22}$$

and

$$A_k = \frac{\gamma_k - 1}{\gamma_k} \frac{\rho_k \alpha_k c_{p_k}}{\sum \rho_k \alpha_k c_{p_k}}, \tag{5.23}$$

$$z = \sum \rho_k \alpha_k e_k + p - \sum \rho_k \alpha_k e_{*_k}, \tag{5.24}$$

$$q_k = p_{\infty_k} - \sum \rho_k \alpha_k e_k + \sum \rho_k \alpha_k e_{*_k}, \tag{5.25}$$

$$h = \frac{1}{z} + \frac{1}{p + \min_k p_{\infty_k}}, \tag{5.26}$$

converges monotonically and quadratically to the unique physically valid solution p. Once the pressure is known, the rest of the demanded variables can be directly calculated.

5.4 Approximate eigenvalues

In order to calculate the eigenvalues, one must rewrite the system (5.18) in the quasilinear form

$$\frac{\partial U}{\partial t} + A\left(U\right)\frac{\partial U}{\partial x} = S\left(U\right), \tag{5.27}$$

so that the Jacobian matrix and its associated eigenvalues can be analytically calculated. This could lead to complicated expressions and, therefore, it is preferable to take approximate eigenvalues. For the Lax-Friedrichs scheme, the eigenvalues deduced from the four-equation model (valid only to low order in $v_g - v_l$) are going to be taken as approximate eigenvalues for the five-equation model in order to estimate the time step Δt. According to [1], the eigenvalues corresponding to the system of four balance laws can be written as

$$\lambda^{\mathrm{p}} = \bar{v}^{\mathrm{p}} \pm \hat{c} \tag{5.28}$$

for the pressure waves and

$$\lambda^{\mathrm{v}} = \bar{v}^{\mathrm{v}} \pm \beta \tag{5.29}$$

for the volume fraction waves. The following expressions are utilised:

$$v^{\mathrm{p}} = \frac{\rho_g\alpha_l v_l + \rho_l\alpha_g v_g}{\rho_g\alpha_l + \rho_l\alpha_g}, \tag{5.30}$$

$$v^{\mathrm{v}} = \frac{\rho_g\alpha_l v_g + \rho_l\alpha_g v_l}{\rho_g\alpha_l + \rho_l\alpha_g}, \tag{5.31}$$

$$\beta = \sqrt{\frac{\delta p\left(\rho_g\alpha_l + \rho_l\alpha_g\right) - \rho_l\alpha_l\rho_g\alpha_g(v_g - v_l)^2}{\left(\rho_g\alpha_l + \rho_l\alpha_g\right)^2}}, \tag{5.32}$$

together with an approximate mixture sound velocity given by

$$\hat{c} = \sqrt{\frac{\rho_l\alpha_g + \rho_g\alpha_l}{\left(\partial\rho_g/\partial p\right)_s\rho_l\alpha_g + \left(\partial\rho_l/\partial p\right)_s\rho_g\alpha_l}}. \tag{5.33}$$

5.5 Jacobian matrix

As one can see, an analytical expression for the Jacobian matrix must be found to be able to obtain the eigenvalues associated with the system (5.18). Another reason to find this matrix comes from the fact that it will be used later in other numerical methods like the Roe method in which the Jacobian and the Roe matrices are related.

When the nonconservative system (5.18) is written in quasilinear form (5.27), the following expression for the Jacobian matrix

$$A\left(U\right) = \frac{\partial F}{\partial U} + B\frac{\partial W}{\partial U} \tag{5.34}$$

can be found.

5.5.1 Simplified notation

It is convenient to rewrite the expressions (5.19) using a more convenient notation based on the definitions of the volumetric mass

$$m_k = \rho_k \alpha_k, \tag{5.35}$$

and the volumetric momentum

$$I_k = \rho_k \alpha_k v_k, \tag{5.36}$$

for each phase:

$$U = \begin{bmatrix} m_g \\ m_l \\ I_g \\ I_l \\ E \end{bmatrix}, \quad F(U) = \begin{bmatrix} I_g \\ I_l \\ I_g v_g + \alpha_g \delta p \\ I_l v_l + \alpha_l \delta p \\ E_g v_g + E_l v_l + p\left(\alpha_g v_g + \alpha_l v_l\right) \end{bmatrix},$$

$$B(U) = \begin{bmatrix} 0 & 0 \\ 0 & 0 \\ \alpha_g & -\alpha_g \\ \alpha_l & -\alpha_l \\ 0 & 0 \end{bmatrix}, \quad W(U) = \begin{bmatrix} p \\ \delta p \end{bmatrix}, \tag{5.37}$$

$$S(U) = \begin{bmatrix} 0 \\ 0 \\ m_g g_x \\ m_l g_x \\ \left(I_g + I_l\right) g_x \end{bmatrix}.$$

5.5.2 Differentials

The method utilised in this work to calculate A consists on expressing the variables located in the rows of F and BW in terms of the conserved variables U, so that the differentiation presented in (5.34) can be easily performed.

The derivatives of the conserved variables can be expressed as a vector

$$\mathrm{d}U = \begin{bmatrix} \mathrm{d}u_1 \\ \mathrm{d}u_2 \\ \mathrm{d}u_3 \\ \mathrm{d}u_4 \\ \mathrm{d}u_5 \end{bmatrix} = \begin{bmatrix} \mathrm{d}m_g \\ \mathrm{d}m_l \\ \mathrm{d}I_g \\ \mathrm{d}I_l \\ \mathrm{d}E \end{bmatrix}. \tag{5.38}$$

Furthermore, using the relation

$$\mathrm{d}I_k = \mathrm{d}m_k v_k + m_k \mathrm{d}v_k, \tag{5.39}$$

one can obtain the derivatives of the velocities of each phase as a function of the conserved variables:

$$\mathrm{d}v_g = \frac{\mathrm{d}u_3 - v_g \mathrm{d}u_1}{m_g}, \tag{5.40}$$

$$\mathrm{d}v_l = \frac{\mathrm{d}u_4 - v_l \mathrm{d}u_2}{m_l}. \tag{5.41}$$

With this information, one can easily obtain the two first rows of the Jacobian matrix. However, the other rows, corresponding to the momentum and energy equations, require some additional work.

Consider now the third and fourth rows of (5.34). These rows correspond to the conservative and non-conservative flux terms related to the momentum equations of the system (5.18), for the gas phase and liquid phase respectively.

For the gas, the third row may be written as

$$\left(\frac{\partial F}{\partial U}+B\frac{\partial W}{\partial U}\right)_3 = I_g\nabla v_g + v_g\nabla I_g + \delta p\nabla\alpha_g + \alpha_g\nabla p, \tag{5.42}$$

where the operator *gradient of a scalar* has been introduced

$$\nabla(\cdot) = \begin{bmatrix} \partial(\cdot)/\partial u_1 \\ \vdots \\ \partial(\cdot)/\partial u_p \\ \vdots \\ \partial(\cdot)/\partial u_5 \end{bmatrix}. \tag{5.43}$$

An analogous expression is obtained for the liquid phase

$$\left(\frac{\partial F}{\partial U}+B\frac{\partial W}{\partial U}\right)_4 = I_l\nabla v_l + v_l\nabla I_l + \delta p\nabla\alpha_l + \alpha_l\nabla p. \tag{5.44}$$

The fifth row of (5.34) corresponds to the energy equation of (5.18) and may be expressed as

$$\begin{aligned}\left(\frac{\partial F}{\partial U}+B\frac{\partial W}{\partial U}\right)_5 = {} & E_g\nabla v_g + v_g\left\{\left(e_g+\frac{1}{2}v_g^2\right)\nabla m_g + m_g\left(\nabla e_g + v_g\nabla v_g\right)\right\} \\ & + E_l\nabla v_l + v_l\left\{\left(e_l+\frac{1}{2}v_l^2\right)\nabla m_l + m_l\left(\nabla e_l + v_l\nabla v_l\right)\right\} \\ & + \left(\alpha_g v_g + \alpha_l v_l\right)\nabla p + p\left\{\alpha_g\nabla v_g + \alpha_l\nabla v_l + \left(v_g - v_l\right)\nabla\alpha_g\right\},\end{aligned} \tag{5.45}$$

where the total energy of each phase has been decomposed into internal energy and kinetic energy. The property (5.10) has been used as well.

5.5.3 Thermodynamic considerations

As the reader can imagine, one should express the differentials of e_g, e_l, α_g and p as a function of the conserved variables and, consequently, thermodynamic relations must be considered.

General equations of state will be considered in this work. In particular, two independent EOSes are introduced

$$\rho_k = \rho_k(T,p), \tag{5.46}$$

$$e_k = e_k(T,\rho_k), \tag{5.47}$$

and therefore, their differentials

$$\mathrm{d}\rho_k = \left.\frac{\partial\rho_k}{\partial T}\right|_p \mathrm{d}T + \left.\frac{\partial\rho_k}{\partial p}\right|_T \mathrm{d}p, \tag{5.48}$$

$$\mathrm{d}e_k = \left.\frac{\partial e_k}{\partial T}\right|_{\rho_k} \mathrm{d}T + \left.\frac{\partial e_k}{\partial \rho_k}\right|_T \mathrm{d}\rho_k. \tag{5.49}$$

It would be convenient to introduce some simplifications for these two last relations

$$a_k = \left.\frac{\partial \rho_k}{\partial T}\right|_p, \quad b_k = \left.\frac{\partial \rho_k}{\partial p}\right|_T, \quad c_k = \left.\frac{\partial e_k}{\partial T}\right|_{\rho_k}, \quad d_k = \left.\frac{\partial e_k}{\partial \rho_k}\right|_T. \tag{5.50}$$

In the particular case that the stiffened gas EOS is considered for both phases, the partial derivatives (5.50) may be written as

$$a_k = -\frac{p_k + p_{\infty_k}}{(\gamma_k - 1)\, c_{v_k} T^2}, \tag{5.51}$$

$$b_k = \frac{1}{(\gamma_k - 1)\, c_{v_k} T}, \tag{5.52}$$

$$c_k = c_{v_k}, \tag{5.53}$$

$$d_k = -\frac{p_{\infty_k}}{\rho_k^2}. \tag{5.54}$$

5.5.4 Closure considerations

The problem of finding $\mathrm{d}e_g$, $\mathrm{d}e_l$, $\mathrm{d}\alpha_g$ and $\mathrm{d}p$ requires, apart from the previous thermodynamic relations (5.48)-(5.49), two additional equations.

In particular, the following expression for the total energy must be used

$$m_g \mathrm{d}e_g + m_l \mathrm{d}e_l = \mathrm{d}u_5 - \left(e_g - \frac{1}{2}v_g^2\right)\mathrm{d}u_1 - \left(e_l - \frac{1}{2}v_l^2\right)\mathrm{d}u_2 - v_g \mathrm{d}u_3 - v_l \mathrm{d}u_4. \tag{5.55}$$

Another expression to be utilised comes from (5.10) which can also be expressed as $\mathrm{d}\left(\alpha_g + \alpha_l\right) = 0$. However, it is more convenient to write this equation as

$$\frac{\mathrm{d}u_1}{\rho_g} + \frac{\mathrm{d}u_2}{\rho_l} = q\mathrm{d}T + r\mathrm{d}p, \tag{5.56}$$

where

$$q = \sum_k \frac{\alpha_k a_k}{\rho_k}, \quad r = \sum_k \frac{\alpha_k b_k}{\rho_k}. \tag{5.57}$$

The resolution of the system of equations given by the relations (5.48)-(5.49), (5.55) and (5.56) allows to express the differentials $\mathrm{d}\rho_g$, $\mathrm{d}\rho_l$, $\mathrm{d}e_g$, $\mathrm{d}e_l$, $\mathrm{d}T$ and $\mathrm{d}p$ as functions of the derivatives of the conserved variables $\mathrm{d}U$.

The final results of this system may be written in the form of gradients

$$\nabla\rho_g = \lambda^{-1}\begin{bmatrix} \dot{v}_g^2 x_g + (\eta_2 - b_g \sum_k m_k c_k)/\rho_g \\ \dot{v}_l^2 x_g + (\eta_2 - b_g \sum_k m_k c_k)/\rho_l \\ -v_g x_g \\ -v_l x_g \\ x_g \end{bmatrix}, \tag{5.58}$$

$$\nabla p = \lambda^{-1}\begin{bmatrix} \dot{v}_g^2 q - \sum_k m_k (a_k d_k + c_k)/\rho_g \\ \dot{v}_l^2 q - \sum_k m_k (a_k d_k + c_k)/\rho_l \\ -v_g q \\ -v_l q \\ q \end{bmatrix}, \tag{5.59}$$

$$\nabla e_g = \lambda^{-1}\begin{bmatrix} \dot{v}_g^2 z_g + (d_g \eta_2 + m_l \xi)/\rho_g \\ \dot{v}_l^2 z_g + (d_g \eta_2 + m_l \xi)/\rho_l \\ -v_g z_g \\ -v_l z_g \\ z_g \end{bmatrix}, \tag{5.60}$$

$$\nabla e_l = \lambda^{-1}\begin{bmatrix} \dot{v}_g^2 z_l + (d_l \eta_1 - m_g \xi)/\rho_g \\ \dot{v}_l^2 z_l + (d_l \eta_1 - m_g \xi)/\rho_l \\ -v_g z_l \\ -v_l z_l \\ z_l \end{bmatrix}, \tag{5.61}$$

where

$$\lambda = -r \sum_k m_k (a_k d_k + c_k) + q \sum_k m_k b_k d_k, \tag{5.62}$$

$$\dot{v}_k^2 = \frac{1}{2} v_k^2 - e_k, \tag{5.63}$$

$$x_k = -a_k r + b_k q, \tag{5.64}$$

$$z_k = -r (a_k d_k + c_k) + q b_k d_k, \tag{5.65}$$

$$\xi = c_g b_l d_l - c_l b_g d_g, \tag{5.66}$$

$$\eta_1 = m_g d_g (a_l b_g - a_g b_l), \tag{5.67}$$

$$\eta_2 = m_l d_l (a_g b_l - a_l b_g). \tag{5.68}$$

For the gas volume fraction, it is recommendable to use the definition of m_g

$$\nabla\alpha_g = -\nabla\alpha_l = \frac{\mathrm{d}u_1}{\rho_g}\begin{bmatrix} 1 \\ 0 \\ 0 \\ 0 \\ 0 \end{bmatrix} - \frac{\alpha_g}{\rho_g}\nabla\rho_g. \tag{5.69}$$

Finally, the differentials are obtained by application of the definition of the gradient

$$\mathrm{d}(\cdot) = \nabla(\cdot) \cdot \mathrm{d}U. \tag{5.70}$$

5.5.5 Analytical expressions

Now it is possible to fully determine the Jacobian matrix. This matrix has been split into one convective matrix and two pressure matrices

$$A = A_c + A_{p_1} + A_{p_2}. \tag{5.71}$$

Using the notation

$$\mathrm{d}\left(\cdot\right) = \sum_{p=1}^{5} \left(\cdot\right)_p \mathrm{d}u_p \tag{5.72}$$

for the partial derivatives of ρ_g, ρ_l, e_g, e_l, T, p and α_p, the convective matrix may be written as

$$A_c = \begin{bmatrix} 0 & 0 & 1 & 0 & 0 \\ 0 & 0 & 0 & 1 & 0 \\ -v_g^2 & 0 & 2v_g & 0 & 0 \\ 0 & -v_l^2 & 0 & 2v_l & 0 \\ a_{c_1} & a_{c_2} & a_{c_3} & a_{c_4} & a_{c_5} \end{bmatrix}, \tag{5.73}$$

where

$$a_{c_1} = I_g e_{g_1} + I_l e_{l_1} - v_g^3, \tag{5.74}$$
$$a_{c_2} = I_g e_{g_2} + I_l e_{l_2} - v_l^3, \tag{5.75}$$
$$a_{c_3} = e_g + \frac{3}{2} v_g^2 + I_g e_{g_3} + I_l e_{l_3}, \tag{5.76}$$
$$a_{c_4} = e_l + \frac{3}{2} v_l^2 + I_g e_{g_4} + I_l e_{l_4}, \tag{5.77}$$
$$a_{c_5} = I_g e_{g_5} + I_l e_{l_5}. \tag{5.78}$$

The pressure matrices may be written as

$$A_{p_1} = \frac{\delta p \alpha_g}{\rho_g} \begin{bmatrix} 0 & 0 & 0 & 0 & 0 \\ 0 & 0 & 0 & 0 & 0 \\ 1/\alpha_g - \rho_{g_1} & -\rho_{g_2} & -\rho_{g_3} & -\rho_{g_4} & -\rho_{g_5} \\ \rho_{g_1} - 1/\alpha_g & \rho_{g_2} & \rho_{g_3} & \rho_{g_4} & \rho_{g_5} \\ 0 & 0 & 0 & 0 & 0 \end{bmatrix}, \tag{5.79}$$

$$A_{p_2} = \begin{bmatrix} 0 & 0 & 0 & 0 & 0 \\ 0 & 0 & 0 & 0 & 0 \\ \alpha_g p_1 & \alpha_g p_2 & \alpha_g p_3 & \alpha_g p_4 & \alpha_g p_5 \\ \alpha_l p_1 & \alpha_l p_2 & \alpha_l p_3 & \alpha_l p_4 & \alpha_l p_5 \\ a_{p_1} & a_{p_2} & a_{p_3} & a_{p_4} & a_{p_5} \end{bmatrix}, \tag{5.80}$$

where

$$a_{p_1} = \sum_k \alpha_k v_k p_1 - p\left(\frac{v_g}{\rho_g} + \frac{(v_g - v_l)\,\alpha_g \rho_{g_1}}{\rho_g}\right), \tag{5.81}$$

$$a_{p_2} = \sum_k \alpha_k v_k p_2 - p\left(\frac{v_l}{\rho_l} + \frac{(v_g - v_l)\,\alpha_g \rho_{g_2}}{\rho_g}\right), \tag{5.82}$$

$$a_{p_3} = \sum_k \alpha_k v_k p_3 + p\left(\frac{1}{\rho_g} + \frac{(v_g - v_l)\,\alpha_g \rho_{g_3}}{\rho_g}\right), \tag{5.83}$$

$$a_{p_4} = \sum_k \alpha_k v_k p_4 + p\left(\frac{1}{\rho_l} + \frac{(v_g - v_l)\,\alpha_g \rho_{g_4}}{\rho_g}\right), \tag{5.84}$$

$$a_{p_5} = \sum_k \alpha_k v_k p_5 - p\frac{(v_g - v_l)\,\alpha_g \rho_{g_5}}{\rho_g}. \tag{5.85}$$

5.6 Roe matrix

The Roe matrix can be obtained using the same procedure described for the Jacobian matrix.

The method based on *direct algebraic manipulation* described in Section 2.5.1 has been utilised since the introduction of a energy equation for the mixture complicates the obtaining of a *parameter vector*. Therefore, relations (2.19)-(2.22) have been used along with the third condition of Roe:

$$\hat{A}_{i-1/2}\left(U_i - U_{i-1}\right) = F\left(U_i\right) - F\left(U_{i-1}\right). \tag{5.86}$$

It is important to clarify that the Roe matrix is an average matrix and therefore one should be careful in the treatment of the arithmetic averages $(\bar{\cdot})$ and the geometric averages $(\tilde{\cdot})$.

5.6.1 Differentials

In order to simplify the notation, it would be convenient to introduce the operator Δ to indicate a *jump* in a variable. Applied to the column vector of the conserved variables U yields

$$\Delta U = U_i - U_{i-1}, \tag{5.87}$$

and therefore the third condition of Roe can be rewritten as

$$\hat{A}_{i-1/2}\Delta U = \Delta F. \tag{5.88}$$

While the derivatives of the conserved variables were necessary to obtain the Jacobian matrix, the Roe matrix requires the derivatives of the jumps of the conserved variables

$$\mathrm{d}\Delta U = \begin{bmatrix} \mathrm{d}\Delta u_1 \\ \mathrm{d}\Delta u_2 \\ \mathrm{d}\Delta u_3 \\ \mathrm{d}\Delta u_4 \\ \mathrm{d}\Delta u_5 \end{bmatrix} = \begin{bmatrix} \mathrm{d}\Delta m_g \\ \mathrm{d}\Delta m_l \\ \mathrm{d}\Delta I_g \\ \mathrm{d}\Delta I_l \\ \mathrm{d}\Delta E \end{bmatrix}. \tag{5.89}$$

The discrete variants of the differential rules for rational functions (2.19)-(2.22) have to be taken into account and consequently the relation (5.39) must be expressed as

$$\mathrm{d}\Delta I_k = \mathrm{d}\Delta m_k \overline{v}_k + \overline{m}_k \mathrm{d}\Delta v_k, \tag{5.90}$$

leading to the following expressions for the velocities of each phase:

$$\mathrm{d}\Delta v_g = \frac{\mathrm{d}\Delta u_3 - \overline{v}_g \mathrm{d}\Delta u_1}{\overline{m}_g} \tag{5.91}$$

$$\mathrm{d}\Delta v_l = \frac{\mathrm{d}\Delta u_4 - \overline{v}_l \mathrm{d}\Delta u_2}{\overline{m}_l}. \tag{5.92}$$

Equations (5.42), (5.44) and (5.45) may be rewritten as

$$\left(\frac{\partial \Delta F}{\partial \Delta U} + \overline{\overline{B}}\frac{\partial \Delta W}{\partial \Delta U}\right)_3 = \overline{I}_g \nabla(\Delta v_g) + \overline{v}_g \nabla(\Delta I_g) + \overline{\overline{\delta p}} \nabla(\Delta \alpha_g) + \overline{\overline{\alpha}}_g \nabla(\Delta p), \tag{5.93}$$

$$\left(\frac{\partial \Delta F}{\partial \Delta U} + \overline{\overline{B}}\frac{\partial \Delta W}{\partial \Delta U}\right)_4 = \overline{I}_l \nabla(\Delta v_l) + \overline{v}_l \nabla(\Delta I_l) + \overline{\overline{\delta p}} \nabla(\Delta \alpha_l) + \overline{\overline{\alpha}}_l \nabla(\Delta p), \tag{5.94}$$

$$\begin{aligned}
&\left(\frac{\partial \Delta F}{\partial \Delta U} + \overline{\overline{B}}\frac{\partial \Delta W}{\partial \Delta U}\right)_5 = \\
&\overline{E}_g \nabla(\Delta v_g) + \overline{v}_g \left\{ \overline{e_g + \frac{1}{2} v_g^2} \nabla(\Delta m_g) + \overline{m}_g \Big(\nabla(\Delta e_g) + \overline{v}_g \nabla(\Delta v_g) \Big) \right\} \\
&\overline{E}_l \nabla(\Delta v_l) + \overline{v}_l \left\{ \overline{e_l + \frac{1}{2} v_l^2} \nabla(\Delta m_l) + \overline{m}_l \Big(\nabla(\Delta e_l) + \overline{v}_l \nabla(\Delta v_l) \Big) \right\} \\
&+ \overline{\alpha_g v_g + \alpha_l v_l} \nabla(\Delta p) + \overline{p} \Big\{ \overline{\alpha}_g \nabla(\Delta v)_g + \overline{\alpha}_l \nabla(\Delta v_l) + \overline{v_g - v_l} \nabla(\Delta \alpha_g) \Big\}.
\end{aligned} \tag{5.95}$$

where $\overline{(\cdot)}$ represents the average over a certain formally consistent path as described in Section 2.7.

5.6.2 Thermodynamic considerations

Relations (5.48)-(5.49) become

$$\mathrm{d}\Delta \rho_k = \left.\frac{\partial \Delta \rho_k}{\partial \Delta T}\right|_{\Delta p} \mathrm{d}\Delta T + \left.\frac{\partial \Delta \rho_k}{\partial \Delta p}\right|_{\Delta T} \mathrm{d}\Delta p, \tag{5.96}$$

$$\mathrm{d}\Delta e_k = \left.\frac{\partial \Delta e_k}{\partial \Delta T}\right|_{\Delta \rho_k} \mathrm{d}\Delta T + \left.\frac{\partial \Delta e_k}{\partial \Delta \rho_k}\right|_{\Delta T} \mathrm{d}\Delta \rho_k. \tag{5.97}$$

Using the same simplifications that those introduced in (5.50), the following expressions are obtained for the particular case of the stiffened gas equation of state applied to the phases

$$\hat{a}_k = -\frac{\overline{p}_k + p_{\infty_k}}{(\gamma_k - 1)\, c_{v_k} \widetilde{\overline{T}}^2}, \tag{5.98}$$

$$\hat{b}_k = \frac{1}{(\gamma_k - 1)\, c_{v_k} \overline{T}}, \tag{5.99}$$

$$\hat{c}_k = c_{v_k}, \tag{5.100}$$

$$\hat{d}_k = -\frac{p_{\infty_k}}{\tilde{\rho}_k^2}. \tag{5.101}$$

5.6.3 Closure considerations

Two additional equations must be introduced in order to find the differentials of Δe_g, Δe_l, $\Delta\alpha_g$ and Δp. Thus, the average of the total energy equation (5.55) may be expressed as

$$\overline{m}_g \mathrm{d}\Delta e_g + \overline{m}_l \mathrm{d}\Delta e_l = \mathrm{d}\Delta u_5 - \widehat{v_g^2}\mathrm{d}\Delta u_1 - \widehat{v_l^2}\mathrm{d}\Delta u_2 - \overline{v}_g \mathrm{d}\Delta u_3 - \overline{v}_l \mathrm{d}\Delta u_4, \tag{5.102}$$

where

$$\widehat{v_k^2} = \overline{v}_k^2 - \frac{1}{2}\overline{v_k^2} - \overline{e}_k. \tag{5.103}$$

And the average of equation (5.56) may be rewritten as

$$\frac{\mathrm{d}\Delta u_1}{\overline{\rho}_g} + \frac{\mathrm{d}\Delta u_2}{\overline{\rho}_l} = \hat{q}\mathrm{d}\Delta T + \hat{r}\mathrm{d}\Delta p, \tag{5.104}$$

where

$$\hat{q} = \sum_k \frac{\overline{\alpha}_k \hat{a}_k}{\overline{\rho}_k}, \quad \hat{r} = \sum_k \frac{\overline{\alpha}_k \hat{b}_k}{\overline{\rho}_k}. \tag{5.105}$$

Finally, the resolution for this problem gives the following expressions, written in the form of gradients:

$$\nabla(\Delta\rho_g) = \hat{\lambda}^{-1}\begin{bmatrix} \widehat{v_g^2}\hat{x}_g + \left(\hat{\eta}_2 - \hat{b}_g \sum_k \overline{m}_k \hat{c}_k\right)/\overline{\rho}_g \\ \widehat{v_l^2}\hat{x}_g + \left(\hat{\eta}_2 - \hat{b}_g \sum_k \overline{m}_k \hat{c}_k\right)/\overline{\rho}_l \\ -\overline{v}_g \hat{x}_g \\ -\overline{v}_l \hat{x}_g \\ \hat{x}_g \end{bmatrix}, \tag{5.106}$$

$$\nabla(\Delta p) = \hat{\lambda}^{-1}\begin{bmatrix} \widehat{v_g^2}\hat{q} - \sum_k \overline{m}_k \left(\hat{a}_k \hat{b}_k + \hat{c}_k\right)/\overline{\rho}_g \\ \widehat{v_l^2}\hat{q} - \sum_k \overline{m}_k \left(\hat{a}_k \hat{b}_k + \hat{c}_k\right)/\overline{\rho}_l \\ -\overline{v}_g \hat{q} \\ -\overline{v}_l \hat{q} \\ \hat{q} \end{bmatrix}, \tag{5.107}$$

$$\nabla(\Delta e_g) = \hat{\lambda}^{-1}\begin{bmatrix} \widehat{v_g^2}\hat{z}_g + \left(\hat{b}_g \hat{\eta}_2 + \overline{m}_l \hat{\xi}\right)/\overline{\rho}_g \\ \widehat{v_l^2}\hat{z}_g + \left(\hat{b}_g \hat{\eta}_2 + \overline{m}_l \hat{\xi}\right)/\overline{\rho}_l \\ -\overline{v}_g \hat{z}_g \\ -\overline{v}_l \hat{z}_g \\ \hat{z}_g \end{bmatrix}, \tag{5.108}$$

$$\nabla(\Delta e_l) = \hat{\lambda}^{-1}\begin{bmatrix} \widehat{v_g^2}\hat{z}_l + \left(\hat{b}_l \hat{\eta}_1 - \overline{m}_g \hat{\xi}\right)/\overline{\rho}_g \\ \widehat{v_l^2}\hat{z}_l + \left(\hat{b}_l \hat{\eta}_1 - \overline{m}_g \hat{\xi}\right)/\overline{\rho}_l \\ -\overline{v}_g \hat{z}_l \\ -\overline{v}_l \hat{z}_l \\ \hat{z}_l \end{bmatrix}, \tag{5.109}$$

where

$$\hat{\lambda} = -\hat{r}\sum_k \overline{m}_k \left(\hat{a}_k\hat{d}_k + \hat{c}_k\right) + \hat{q}\sum_k \overline{m}_k\hat{b}_k\hat{d}_k, \tag{5.110}$$

$$\hat{x}_k = -\hat{a}_k\hat{r} + \hat{b}_k\hat{q}, \tag{5.111}$$

$$\hat{z}_k = -\hat{r}\left(\hat{a}_k\hat{d}_k + \hat{c}_k\right) + \hat{q}\hat{b}_k\hat{d}_k, \tag{5.112}$$

$$\hat{\xi} = \hat{c}_g\hat{b}_l\hat{d}_l - \hat{c}_l\hat{b}_g\hat{d}_g, \tag{5.113}$$

$$\hat{\eta}_1 = \overline{m}_g\hat{d}_g\left(\hat{a}_l\hat{b}_g - \hat{a}_g\hat{b}_l\right), \tag{5.114}$$

$$\hat{\eta}_2 = \overline{m}_l\hat{d}_l\left(\hat{a}_g\hat{b}_l - \hat{a}_l\hat{b}_g\right). \tag{5.115}$$

5.6.4 Analytical expressions

Finally, one should arrive to the expression of the Roe matrix by following the same steps taken in the development of the Jacobian matrix

$$\hat{A} = \hat{A}_c + \hat{A}_{p_1} + \hat{A}_{p_2}, \tag{5.116}$$

where

$$\hat{A}_c = \begin{bmatrix} 0 & 0 & 1 & 0 & 0 \\ 0 & 0 & 0 & 1 & 0 \\ -\overline{I}_g\overline{v}_g/\overline{m}_g & 0 & \overline{I}_g/\overline{m}_g + \overline{v}_g & 0 & 0 \\ 0 & -\overline{I}_l\overline{v}_l/\overline{m}_l & 0 & \overline{I}_l/\overline{m}_l + \overline{v}_l & 0 \\ \hat{a}_{c_1} & \hat{a}_{c_2} & \hat{a}_{c_3} & \hat{a}_{c_4} & \hat{a}_{c_5} \end{bmatrix}, \tag{5.117}$$

with

$$\hat{a}_{c_1} = -\frac{\overline{E}_g\overline{v}_g}{\overline{m}_g} - \overline{v}_g\widehat{v_g^2} + \overline{m}_g\overline{v}_g\Delta e_{g_1} + \overline{m}_l\overline{v}_l\Delta e_{l_1}, \tag{5.118}$$

$$\hat{a}_{c_2} = -\frac{\overline{E}_l\overline{v}_l}{\overline{m}_l} - \overline{v}_l\widehat{v_l^2} + \overline{m}_g\overline{v}_g\Delta e_{g_2} + \overline{m}_l\overline{v}_l\Delta e_{l_2}, \tag{5.119}$$

$$\hat{a}_{c_3} = \frac{\overline{E}_g}{\overline{m}_g} + \overline{v}_g^2 + \overline{m}_g\overline{v}_g\Delta e_{g_3} + \overline{m}_l\overline{v}_l\Delta e_{l_3} \tag{5.120}$$

$$\hat{a}_{c_4} = \frac{\overline{E}_l}{\overline{m}_l} + \overline{v}_l^2 + \overline{m}_g\overline{v}_g\Delta e_{g_4} + \overline{m}_l\overline{v}_l\Delta e_{l_4} \tag{5.121}$$

$$\hat{a}_{c_5} = \overline{m}_g\overline{v}_g\Delta e_{g_5} + \overline{m}_l\overline{v}_l\Delta e_{l_5}. \tag{5.122}$$

Note that a similar notation for the partial derivatives described in equation (5.72) has been employed in this case

$$\mathrm{d}\Delta\left(\cdot\right) = \sum_{p=1}^{5}\Delta\left(\cdot\right)_p\mathrm{d}\Delta u_p. \tag{5.123}$$

The pressure matrices may be written as

$$\hat{A}_{p_1} = \frac{\overline{\overline{\Delta p}\overline{\alpha}_g}}{\overline{\rho}_g}\begin{bmatrix} 0 & 0 & 0 & 0 & 0 \\ 0 & 0 & 0 & 0 & 0 \\ 1/\overline{\alpha}_g - \Delta\rho_{g_1} & -\Delta\rho_{g_2} & -\Delta\rho_{g_3} & -\Delta\rho_{g_4} & -\Delta\rho_{g_5} \\ \Delta\rho_{g_1} - 1/\overline{\alpha}_g & \Delta\rho_{g_2} & \Delta\rho_{g_3} & \Delta\rho_{g_4} & \Delta\rho_{g_5} \\ 0 & 0 & 0 & 0 & 0 \end{bmatrix}, \tag{5.124}$$

$$\hat{A}_{p_2} = \begin{bmatrix} 0 & 0 & 0 & 0 & 0 \\ 0 & 0 & 0 & 0 & 0 \\ \overline{\overline{\alpha}}_g\Delta p_1 & \overline{\overline{\alpha}}_g\Delta p_2 & \overline{\overline{\alpha}}_g\Delta p_3 & \overline{\overline{\alpha}}_g\Delta p_4 & \overline{\overline{\alpha}}_g\Delta p_5 \\ \overline{\overline{\alpha}}_l\Delta p_1 & \overline{\overline{\alpha}}_l\Delta p_2 & \overline{\overline{\alpha}}_l\Delta p_3 & \overline{\overline{\alpha}}_l\Delta p_4 & \overline{\overline{\alpha}}_l\Delta p_5 \\ \hat{a}_{p_1} & \hat{a}_{p_2} & \hat{a}_{p_3} & \hat{a}_{p_4} & \hat{a}_{p_5} \end{bmatrix}, \tag{5.125}$$

where

$$\hat{a}_{p_1} = \overline{\sum_k \alpha_k v_k}\Delta p_1 - \overline{p}\left(\frac{\overline{\alpha}_g\overline{v}_g}{\overline{m}_g} + \overline{v_g - v_l}\frac{\overline{\alpha}_g\Delta\rho_{g_1} - 1}{\overline{\rho_g}}\right), \tag{5.126}$$

$$\hat{a}_{p_2} = \overline{\sum_k \alpha_k v_k}\Delta p_2 - \overline{p}\left(\frac{\overline{\alpha}_l\overline{v}_l}{\overline{m}_l} + \overline{v_g - v_l}\frac{\overline{\alpha}_g\Delta\rho_{g_2}}{\overline{\rho_g}}\right), \tag{5.127}$$

$$\hat{a}_{p_3} = \overline{\sum_k \alpha_k v_k}\Delta p_3 + \overline{p}\left(\frac{\overline{\alpha}_g}{\overline{m}_g} - \overline{v_g - v_l}\frac{\overline{\alpha}_g\Delta\rho_{g_3}}{\overline{\rho_g}}\right), \tag{5.128}$$

$$\hat{a}_{p_4} = \overline{\sum_k \alpha_k v_k}\Delta p_4 + \overline{p}\left(\frac{\overline{\alpha}_l}{\overline{m}_l} - \overline{v_g - v_l}\frac{\overline{\alpha}_g\Delta\rho_{g_4}}{\overline{\rho_g}}\right), \tag{5.129}$$

$$\hat{a}_{p_5} = \overline{\sum_k \alpha_k v_k}\Delta p_5 - \overline{p}\overline{v_g - v_l}\frac{\overline{\alpha}_g\Delta\rho_{g_5}}{\overline{\rho_g}}. \tag{5.130}$$

The reader can check that the Roe matrix converges to the Jacobian matrix when the data in two neighbouring cells are equal, satisfying the second condition of Roe described in Section 2.5.

5.7 Considerations about the Jacobian and Roe matrices

The validity of the Jacobian matrix has been tested numerically and by application of other analytical methods (see Section 3.2 of [8]).

The validity of the Roe matrix has also been verified assuring numerically the equality of the second and third conditions described by Roe (see Section 2.5). In fact, the second condition can be proved directly using the previous expressions for the Jacobian and Roe matrices. The third condition of Roe (equation (5.86)) has been checked numerically. Thus, for the momentum equations, the maximum *absolute* difference between the left term and the right term in expression (5.86) was smaller than 10^{-8}. For the energy equation, this difference was smaller than 10^{-6}.

In the moving discontinuity and Toumi's shock tube tests (which will be presented in the next Section), the velocities of both phases are equal at a certain point (they are always equal in the moving discontinuity problem). As a consequence of

this equality between the velocities, complex eigenvalues have been obtained during the decomposition of the Jacobian and Roe matrices (equation (2.13)). However, the complex parts of these eigenvalues were several orders of magnitude smaller than the real parts and, therefore, ignoring them has verified to work in these tests.

Nevertheless, a deep analysis in these particular cases must be considered. But this study may exceed the contents of this Master's Thesis.

5.8 Numerical simulations

This section presents some benchmarks cases from the literature that have already been studied in [11] using the four- and six-equation models for a two-phase flow.

Different numerical schemes have been tested and convergence simulations have been performed in order to verify the validity of the solutions provided by the five-equation model governed by the stiffened gas EOS. Finally, comparisons between the three models have been made in order to show their differences.

5.8.1 Moving discontinuity

This is a basic benchmark with no source terms present. The initial conditions consist of uniform velocities, temperature and pressure, but there is a jump in the gas volume fraction at the middle of a 12 m long horizontal tube (see Table 5.1). Due to these initial conditions, variations should not be introduced in the velocities or in the pressure.

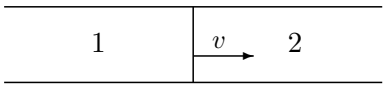

Figure 5.1: The moving discontinuity problem.

Table 5.1: Initial state for the moving-discontinuity problem. Different values of ε were set depending on the numerical scheme used.

Quantity	Symbol (unit)	Left	Right
Gas vol. frac.	$\alpha_g\,(-)$	$1-\varepsilon$	ε
Pressure	$p\,(\mathrm{MPa})$	0.1	0.1
Gas velocity	$v_g\,(\mathrm{m/s})$	100	100
Liq. velocity	$v_l\,(\mathrm{m/s})$	100	100
Temperature	$T\,(\mathrm{K})$	315.9	315.9

The EOS parameters used during the numerical simulations are those given in Table 5.2. The CFL number was set to 0.5. Note that in this particular test, the value σ in equation (5.17) does not have influence because the difference of velocities in (5.17) remains zero at any time.

Convergence of the Lax-Friedrichs scheme

Figure 5.2 shows the convergence of the Lax-Friedrichs scheme at $t = 0.03\,\mathrm{s}$. The value $\varepsilon = 10^{-12}$ was set during these simulations.

Table 5.2: EOS parameters employed in the simulations.

	γ_k $(-)$	p_{∞_k} (Pa)	c_{p_k} $(\mathrm{J\,kg^{-1}\,K^{-1}})$
gas (g)	1.4	0	1008.7
liguid (l)	2.8	8.5×10^8	4186

Ideally the volume fraction should be advected and not smeared, but the Lax-Friedrichs scheme tends to smear the results even for a large number of cells, as illustrated in Figure 5.2(a). On the other hand, Figure 5.2(b) shows how the pressure is not disturbed; in fact, numerical results demonstrated that the order of magnitude of the maximum relative difference of the values of the pressure given by

$$\mathscr{E} = \frac{1}{p^0} \max_{\forall n} \left\{ \left| \max_{\forall i} p_i^n - \min_{\forall i} p_i^n \right| \right\}, \tag{5.131}$$

was about 10^{-8}.

Comparison between different schemes

Figure 5.3 shows the results obtained using the Lax-Friedrichs scheme (LxF), Roe first order and the higher-order extension of Roe using the MC limiter at $t = 0.03\,\mathrm{s}$. Since the Roe method is not as robust as Lax-Friedrichs, the simulations were performed using $\varepsilon = 10^{-1}$. For smaller values of ε the solutions become unstable and only the Lax-Friedrichs scheme can be used.

Additionally, the maximum relative difference of the pressure was calculated for the different schemes. Thus, $\mathscr{E} = 0$ was obtained when the Lax-Friedrichs scheme was utilised. On the other hand, the values $\mathscr{E} \approx 10^{-9}$ and $\mathscr{E} \approx 10^{-10}$ were calculated using the Roe first order scheme and the higher-order extension of Roe, respectively.

5.8.2 Toumi's shock tube

This problem consists of a 100 m tube divided by a membrane at the middle. At $t = 0\,\mathrm{s}$, the membrane ruptures and the flow starts evolving. The initial conditions are given in Table 5.3 and the employed EOS parameters are displayed in Table 5.2. The value $\sigma = 2$ in equation (5.17) was used for this test and the CFL was 0.5. No source terms were considered.

Table 5.3: Initial state for the Toumi's shock tube problem.

Quantity	Symbol (unit)	Left	Right
Gas vol. frac.	$\alpha_g\,(-)$	0.25	0.1
Pressure	$p\,(\mathrm{MPa})$	20	10
Gas velocity	$v_g\,(\mathrm{m/s})$	0	0
Liq. velocity	$v_l\,(\mathrm{m/s})$	0	0
Temperature	$T\,(\mathrm{K})$	308.15	308.15

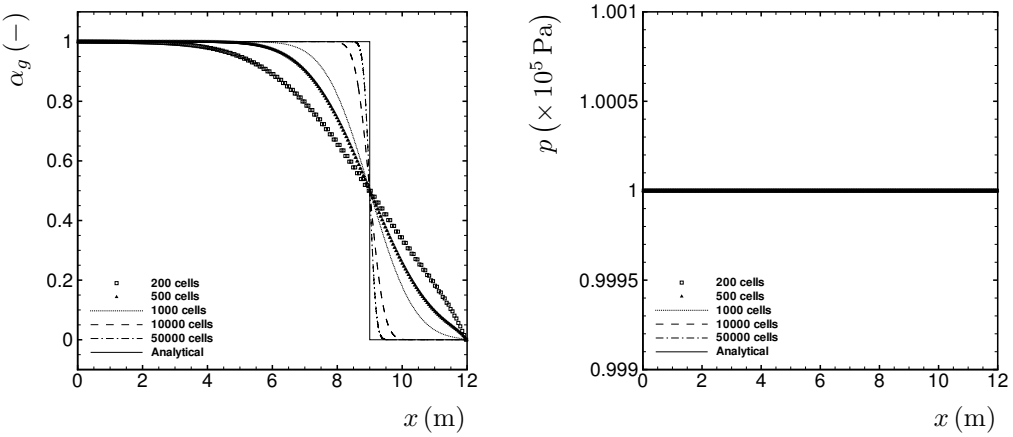

(a) Gas volume fraction. (b) Pressure profiles.

Figure 5.2: Moving discontinuity. Convergence of the Lax-Friedrichs scheme. Results for the gas volume fraction profile (a) and for the pressure profile (b) at $t = 0.03\,\mathrm{s}$ using a CFL number 0.5 and $\varepsilon = 10^{-12}$.

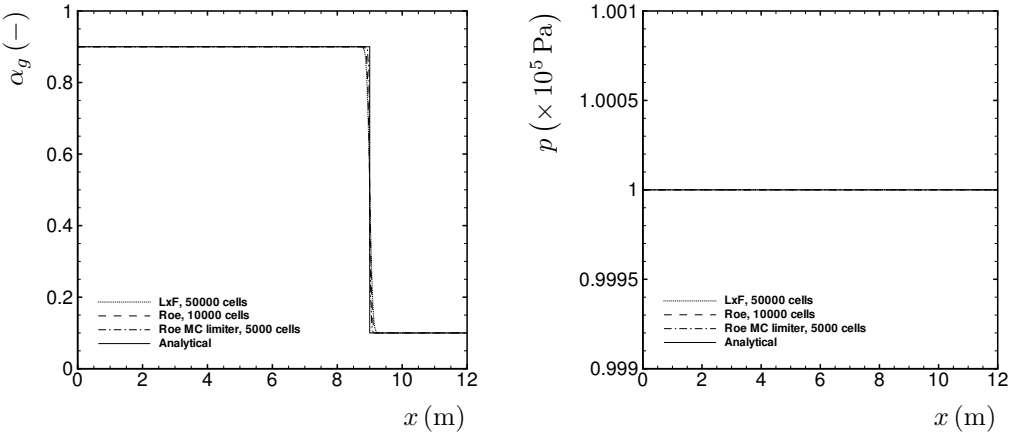

(a) Gas volume fraction. (b) Pressure profiles.

Figure 5.3: Moving discontinuity. Results using the Lax-Friedrichs, Roe first order and Roe with the MC limiter schemes for the gas volume fraction profile (a) and for the pressure profile (b) using a CFL number 0.5 and $\varepsilon = 10^{-1}$ at $t = 0.03\,\mathrm{s}$.

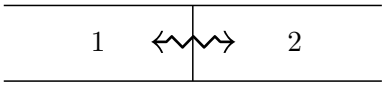

Figure 5.4: Toumi's shock tube problem.

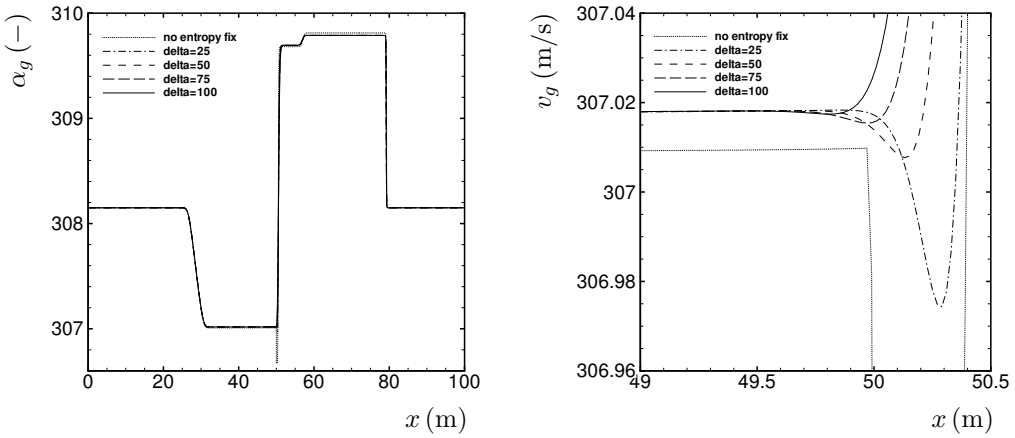

(a) Temperature. (b) Temperature (detail).

Figure 5.5: Toumi's shock tube. Harten's entropy fix applied to the Roe scheme. Results for the temperature at $t = 0.06\,\mathrm{s}$ using a CFL number 0.5. $\delta = 100$ fixes the discontinuity in the middle of the tube.

Convergence of the Roe scheme

A numerical analysis of this problem shows that some eigenvalues associated to the Jacobian matrix are equal to zero at the initial time step. This means that the application of a linearised method like the Roe method may provide unphysically valid solutions, being necessary the use of an entropy fix as discussed in Section 2.5.3. Figure 5.5 shows the necessity of adjusting the parameter δ in relation (2.36). In particular, Figure 5.5(b) shows that the value $\delta = 100$ can be used to avoid this problem without affecting the accuracy of the scheme.

Figure 5.6 shows the convergence of the Roe scheme at $t = 0.06\,\mathrm{s}$ for the gas volume fraction, gas velocity, liquid velocity, temperature and pressure. The results show clearly how the solution converges when the grid gets finer, for the different variables of the problem.

Comparison between different schemes

Figure 5.7 shows the comparision between the Lax-Friedrichs, Roe first order and Roe with the MC limiter schemes.

In order to compare the Roe first order scheme and second order scheme with the MC limiter, an analysis for the error and the order of convergence have been made. The norm of the gas volume fraction is the variable utilised to calculate the error of the scheme

$$||\mathscr{E}(\alpha_g)|| = \Delta x \sum_{\forall i} |\alpha_{g,i} - \alpha_{g,\mathrm{ref},i}|\,, \tag{5.132}$$

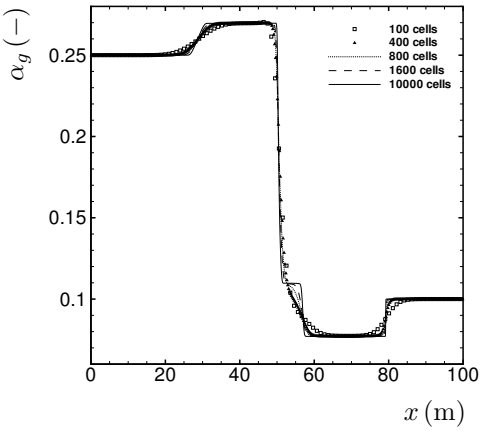

(a) Gas volume fraction.

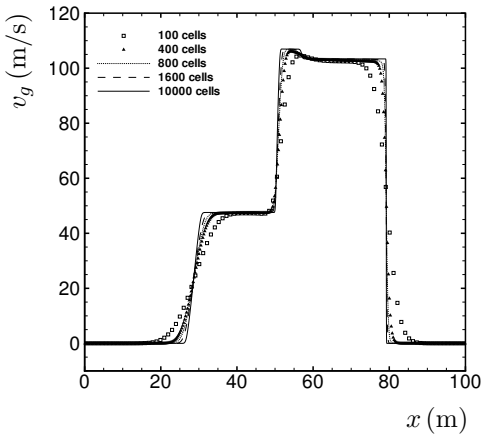

(b) Gas velocity.

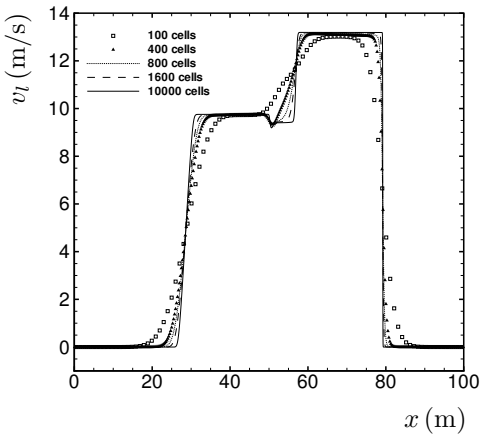

(c) Liquid velocity.

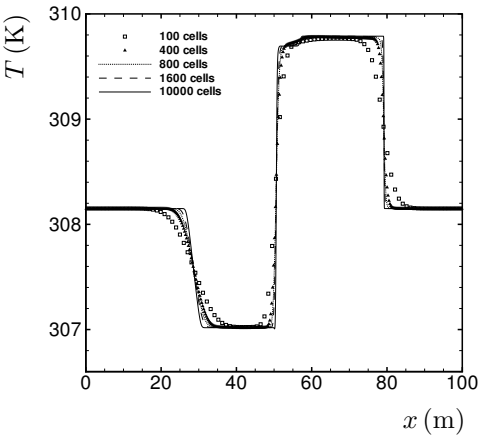

(d) Temperature.

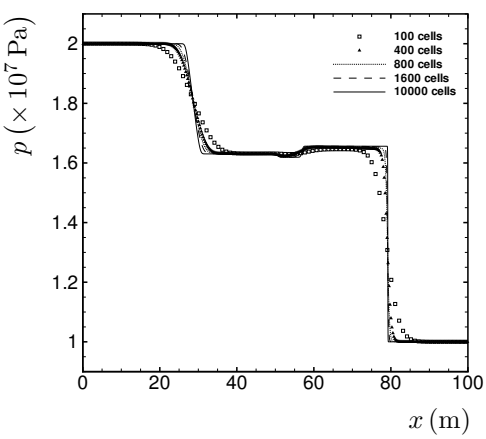

(e) Pressure.

Figure 5.6: Toumi's shock tube. Convergence of the Roe scheme. Results at $t = 0.06\,\mathrm{s}$ using a CFL number 0.5.

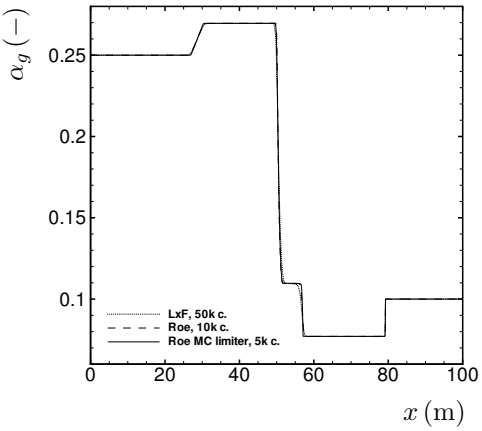

(a) Gas volume fraction.

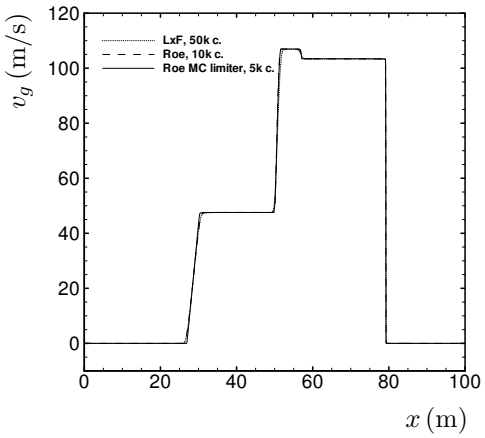

(b) Gas velocity.

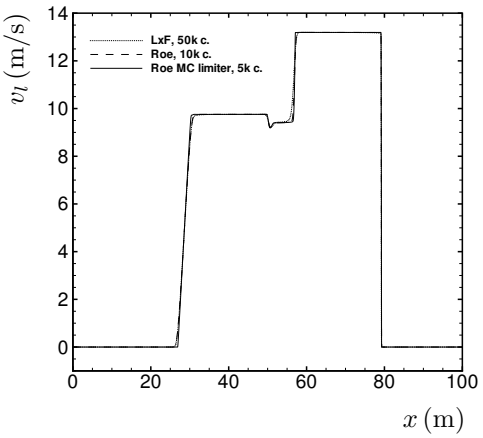

(c) Liquid velocity.

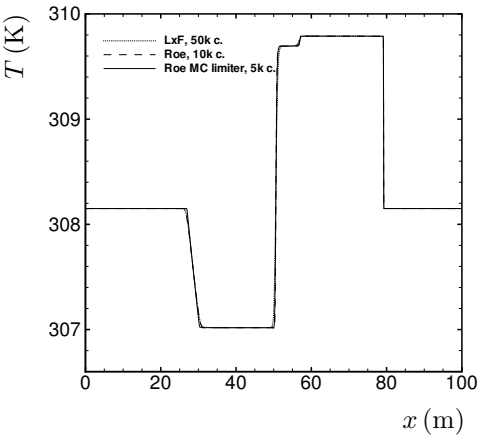

(d) Liquid temperature.

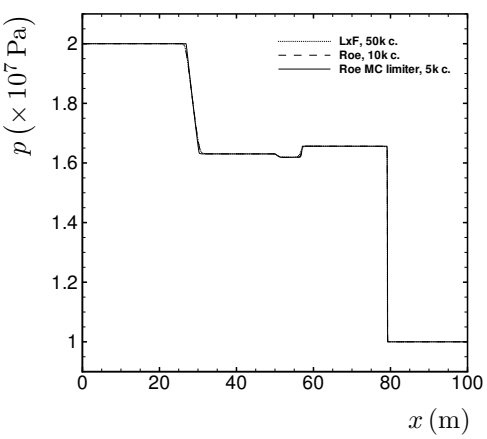

(e) Pressure.

Figure 5.7: Toumi's shock tube. Results for the LxF, Roe first order and Roe with the MC limiter schemes at $t = 0.06\,\mathrm{s}$ using a CFL number 0.5.

whereas the order of the scheme is given by

$$s_n = \frac{\ln\left(||\mathscr{E}(\alpha)||_n / ||\mathscr{E}(\alpha)||_{n-1}\right)}{\ln\left(\Delta x_n / \Delta x_{n-1}\right)}. \tag{5.133}$$

Using as a reference an accurate solution based on a 10000 grid cells, the results for the error and covergence of these schemes are presented in table 5.4.

Table 5.4: Toumi's shock tube problem. Convergence order, s_n, and norm of the error in the gas volume fraction by grid refinement.

	Roe 1^{st} order		Roe 2^{nd} order MC limiter	
Δx (m)	$\|\|\mathscr{E}(\alpha_g)\|\|_n$	s_n	$\|\|\mathscr{E}(\alpha_g)\|\|_n$	s_n
1.0	2.767×10^{-1}	-	2.411×10^{-1}	-
0.5	2.289×10^{-1}	0.27	1.876×10^{-1}	0.36
0.25	1.741×10^{-1}	0.39	1.193×10^{-1}	0.65
0.167	1.369×10^{-1}	0.59	8.882×10^{-2}	0.73
0.125	1.120×10^{-1}	0.70	7.020×10^{-2}	0.82
0.1	9.540×10^{-2}	0.72	5.873×10^{-2}	0.80

As one can see, the convergence of these schemes differs from the theoric values. This is consistent with the fact that the solution of the Toumi's shock tube problem contains shock waves which deteriorate significantly the order of convergence of both schemes.

Comparison between the three models

Figure 5.8 shows a comparison made between the four- and six-equation models resolved by the MUSCL-MUSTA6$_{4-4}$ scheme, using the Van Leer and MC limiters respectively, on a 20000 grid cells extracted from [11] and the five-equation model using the Roe scheme with the MC limiter on a 10000 grid cells.

The results show how the solution of the problem becomes different depending on the model used. Particularly, one should note that the speeds of the travelling waves get slower in the five-equation model. This is consistent with the fact that the five-equation model imposes equal temperatures of both phases, when in the six-equation model the temperature of the gas is much higher than the temperature of the liquid phase. In the five-equation model the temperature practically matches the liquid temperature in the six-equation model, as can be verified in Figure 5.8(d).

On the other hand, for the four-equation model the speeds of sound of both phases have been set, as parameters, close to those obtained in the six-equation model, as described in [11].

In general, for the other variables plotted in Figure 5.8, the five-equation model seems to provide solutions between the four- and the six-equation's.

5.8.3 Water faucet

The water-faucet test constitutes a standard test for one-dimension two-fluid models and methods for their numerical resolution.

Initially, the state in the water faucet is uniform. Values given in Table 5.5 have been taken. At the initial time, gravity is turned on ($g_x = 9.81\,\mathrm{m/s^2}$) and the liquid

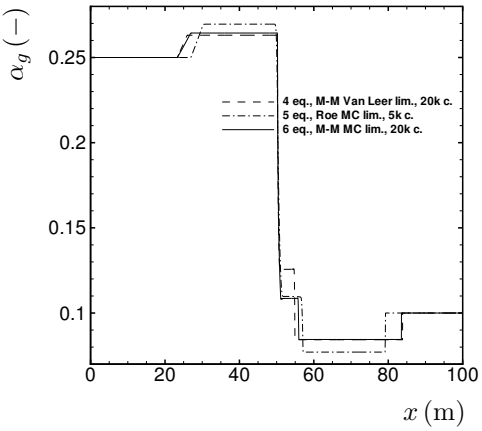

(a) Gas volume fraction.

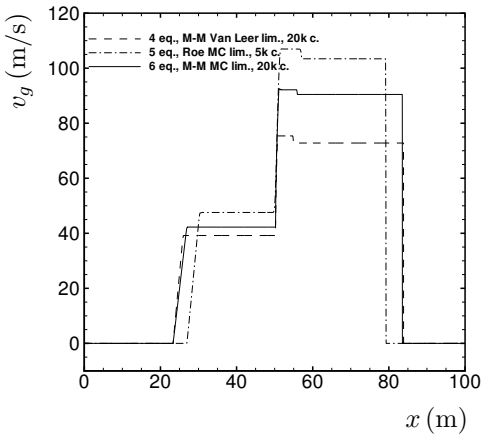

(b) Gas velocity.

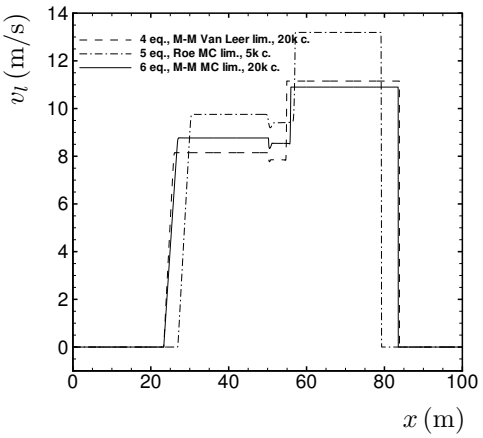

(c) Liquid velocity.

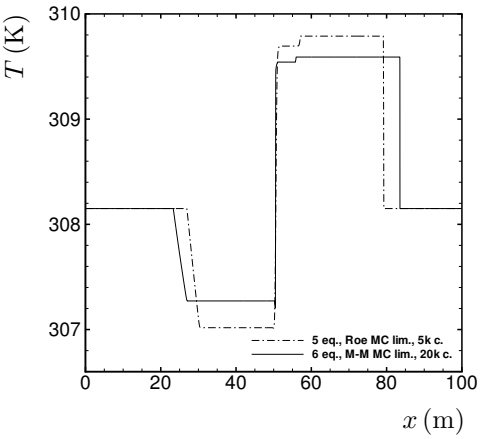

(d) Liquid temperature.

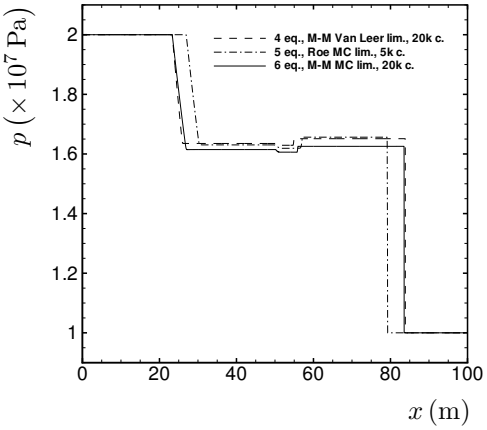

(e) Pressure.

Figure 5.8: Toumi's shock tube. Comparison between the four-, five- and six-equation models. Results at $t = 0.6\,\mathrm{s}$ using a CFL number 0.5.

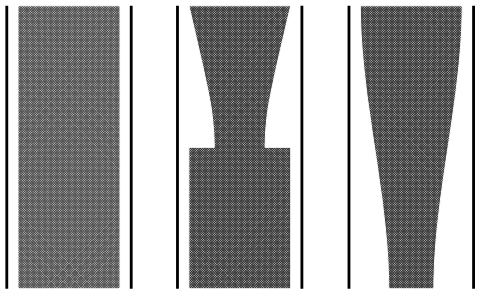

Figure 5.9: The water-faucet-problem.

column starts thinning as a discontinuity moves towards the exit (see Figure 5.9). The results are given at $t = 0.6\,\mathrm{s}$. The CFL number is 0.9 if not otherwise stated. The value $\sigma = 1.2$ in equation (5.17) has been utilised to assure the hyperbolicity of the problem.

Table 5.5: Initial state for the water-faucet test problem.

Quantity	Symbol (unit)	Value
Gas vol. frac.	$\alpha_g\,(-)$	0.2
Pressure	$p\,(\mathrm{MPa})$	0.1
Gas velocity	$v_g\,(\mathrm{m/s})$	0
Liq. velocity	$v_l\,(\mathrm{m/s})$	10.0

Besides, boundary conditions have been imposed:

- inlet boundary conditions are equal to the initial values for the gas volume fraction, and the gas and liquid velocities, as well as for the liquid entropy. The value of the pressure is zeroth order extrapolated;
- a pressure equal to the initial pressure is specified at the outlet. Moreover, the values of the gas volume fraction, the velocities of both phases and the entropy of the liquid are zeroth order extrapolated.

Convergence of the Lax-Friedrichs scheme

Figure 5.10 shows the convergence of the Lax-Friedrichs scheme towards the solution for an increasing number of cells.

Comparison between different schemes

Figure 5.11 shows a comparison made between the Lax-Friedrichs, Roe first order and Roe with the MC limiter schemes.

It is important to notice the lack of accuracy presented by the Lax-Friedrichs scheme: even with a grid ten times more refined, the solutions are less accurate than those provided by the Roe method.

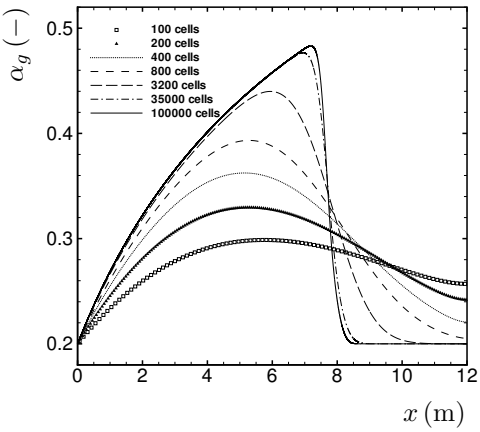

(a) Gas volume fraction.

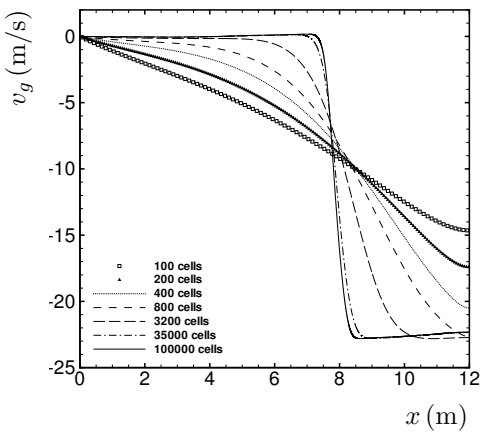

(b) Gas velocity.

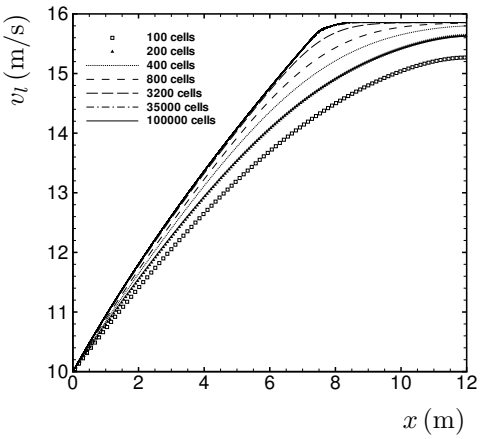

(c) Liquid velocity.

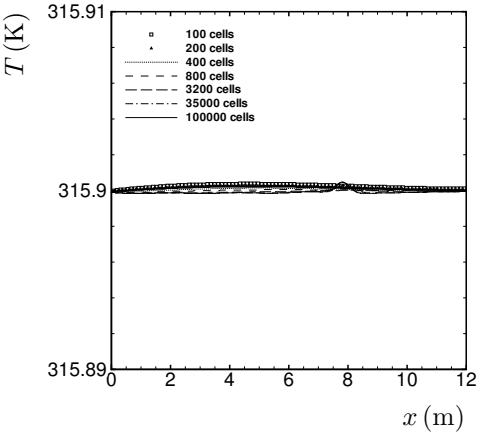

(d) Temperature.

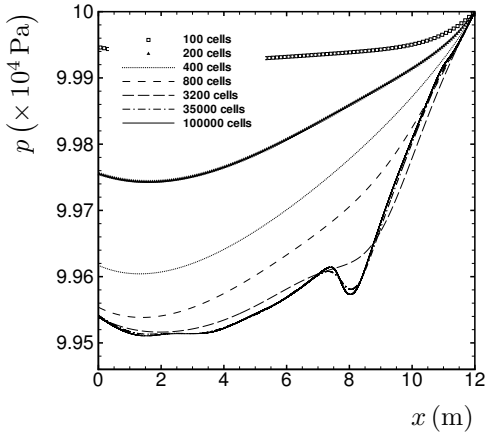

(e) Pressure.

Figure 5.10: Convergence of the water-faucet problem using the Lax-Friedrichs scheme. The CFL number was 0.9. Results at $t = 0.6\,\mathrm{s}$ using a CFL number 0.9.

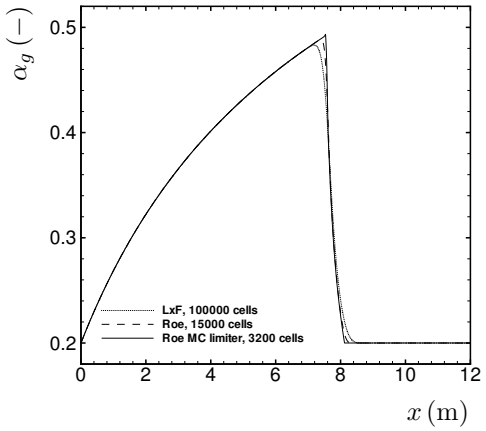

(a) Gas volume fraction.

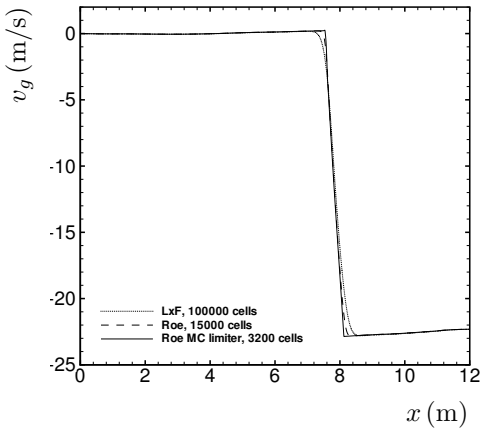

(b) Gas velocity.

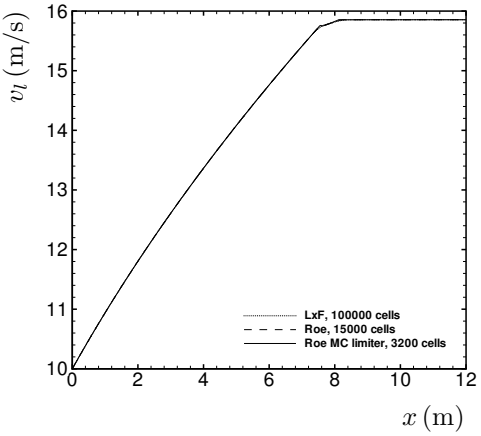

(c) Liquid velocity.

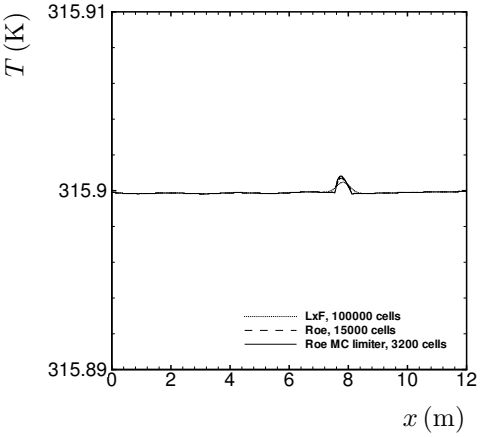

(d) Temperature.

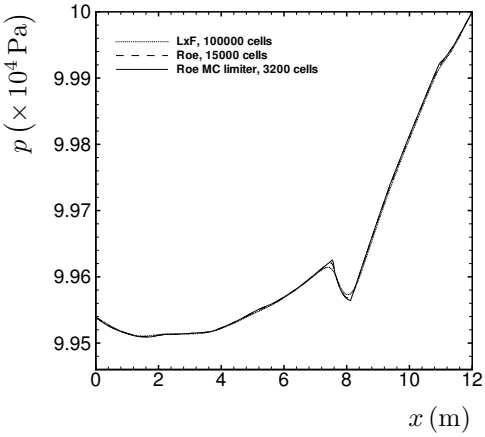

(e) Pressure.

Figure 5.11: Comparison on the solutions provided by different schemes for the water-faucet problem. Results at $t = 0.6\,\mathrm{s}$. The CFL number was 0.9 except when the MC limiter was used, which was changed to 0.5.

Moreover, a study of the order of convergence and the error have been performed for the Roe first order and second order schemes. The results use a solution of 10000 grid cells as a reference and are presented in table 5.6.

Table 5.6: Water-faucet problem. Convergence order, s_n, and norm of the error in the gas volume fraction by grid refinement.

	Roe 1^{st} order		Roe 2^{nd} order MC limiter	
Δx (m)	$\|\|\mathscr{E}(\alpha_g)\|\|_n$	s_n	$\|\|\mathscr{E}(\alpha_g)\|\|_n$	s_n
0.48	4.440×10^{-1}	-	1.432×10^{-1}	-
0.24	5.095×10^{-1}	0.52	5.514×10^{-2}	1.38
0.12	2.019×10^{-1}	0.62	1.866×10^{-2}	1.56
0.06	1.331×10^{-1}	0.60	1.274×10^{-2}	0.55
0.03	8.570×10^{-2}	0.64	5.656×10^{-3}	1.17
0.012	4.515×10^{-2}	0.70	2.075×10^{-3}	1.09

As in the Toumi's shock-tube problem, the results obtained are far from their respetive theoretical values even though no shock waves are presented in the solution. Nevertheless, the solution for the gas volume fraction presented a very sharp profile near $x = 8\,\text{m}$ and consequently a degradation of the order of convergence is expected. On the other hand, these results are closed to those obtained with the Roe scheme for the four-equation model presented in [8].

Comparison between different models

Figure 5.12 shows a comparison made between the four- and six-equation model using the MUSCL-MUSTA6_{4-4} scheme and the five-equation model using the Roe scheme. All the schemes used higher-resolution extension and the MC limiter.

It is possible to appreciate the similitude in the solutions in different variables presented in Figure 5.12, although the pressure seems to be totally different (Figure 5.12(e)). That can be explained also by the fact that the speed of the pressure waves travelling across the domain is slower in the five-equation model compared to the other two. Since the pressure is oscillating in the inlet at a frequency corresponding to the time spent by the pressure waves to go to the outlet and bounce towards the inlet, it is admissible that the instant value of the pressure at that time ($t = 0.6\,\text{s}$) does not correspond to the instant value obtained in the other two models. As well as for the Toumi's shock tube test, the four-equation model has been set using, as parameters, the same sound speeds as those provided by the six-equation model.

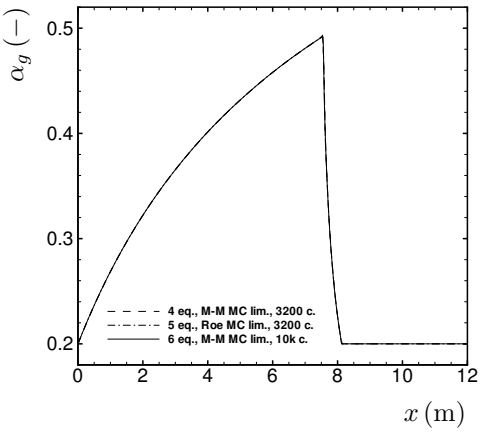

(a) Gas volume fraction.

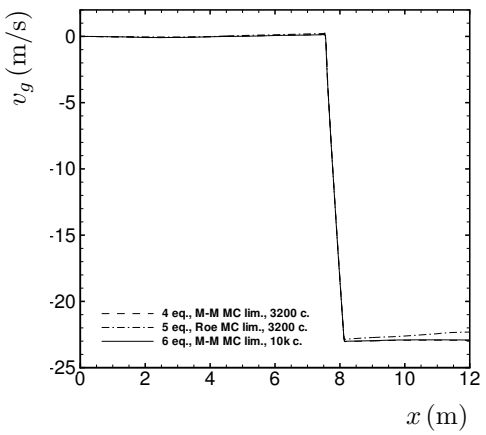

(b) Gas velocity.

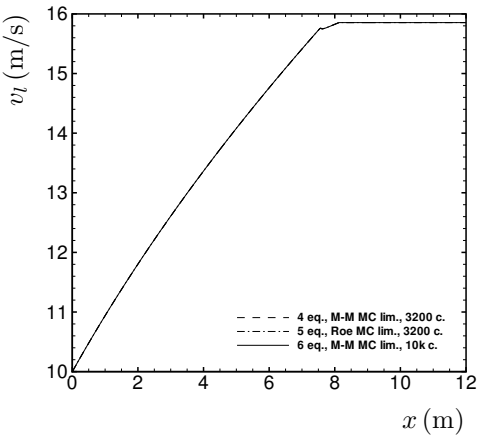

(c) Liquid velocity.

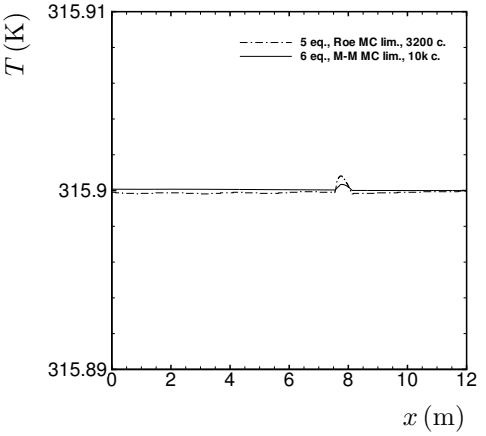

(d) Liquid temperature.

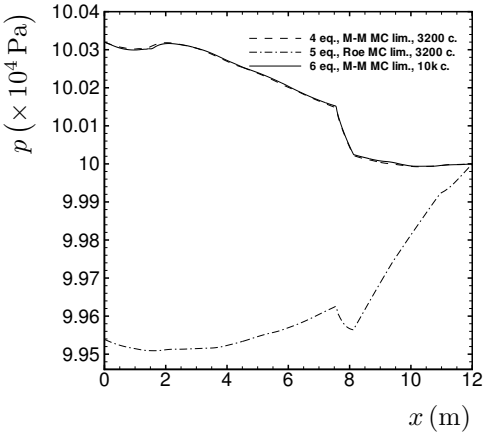

(e) Pressure.

Figure 5.12: Comparison on the solutions provided by the four-, five- and six-equation models for the water-faucet problem. Results at $t = 0.6\,\mathrm{s}$ using a CFL number 0.5.

Chapter 6

Conclusion

The aim of this thesis is the study of two-phases flows. In particular, it has been focused in the development of a five-equation model and the application of several numerical schemes in order to improve its numerical resolution. The final results have been compared to other models previously studied [11].

The results obtained so far have proved that the five-equation model is a good approximation for the study of two-phase flows. The different numerical schemes used have also verified to work satisfactorily on this model. Particularly, the Roe method has demonstrated to be an accurate non expensive numerical scheme.

In the resolution of the moving-discontinuity problem, the parameter $\varepsilon = 10^{-12}$ could be set using the Lax-Friedrichs scheme and it had to be reduced to $\varepsilon = 10^{-1}$ when the Roe scheme was utilised.

Additionally, the water-faucet test have shown that the five-equation model behaves in a similar way that the four- and six-equation models do. The only difference between these models was due to the wave speeds, as it has been discussed previously.

The Toumi's shock tube problem has been resolved after applying the Harten's entropy fix. Differences between the models have also been observed as a consequence of the wave speeds.

Before the end of the Master's Thesis, the writing of a paper regarding this subject has been proposed. This paper will summarize the contents of this work. Additionally, the analytical eigenstructure of the five-equation model will be determined in order to compare the different values of the speed of sound given by different models discussed in this work.

Bibliography

[1] Evje and Flåtten. *Hybrid flux-splitting schemes for a common two-fluid model*. Journal of Computational Physics 192 (2003) 175-210.

[2] Bestion, D. *The physical closure laws in the CATHARE code*. Nucl. Eng. Des., 124 (1990), pp. 229-245.

[3] Flåtten, T., Morin, A. and Munkejord, S. T. *On solutions to equilibrium problems for systems of stiffened gases*. Submitted for publication, 2010.

[4] Flåtten, T., Morin, A. and Munkejord, S. T. *Wave propagation in multicomponent flow models*. SIAM J. Appl. Math., accepted for publication.

[5] Flåtten, T. and Munkejord, S. T. *The approximate Riemann solver of Roe applied to a drift-flux two-phase flow model*. ESAIM: M2AN. Vol. 40, No. 4, 2006, pp. 735-764. DOI: 10.1051/m2an:2006032.

[6] LeVeque, R. J. *Finite Volume Methods for Hyperbolic Problems*. Cambridge texts in applied mathematics, 2002.

[7] Morin, A., Aursand, P. K., Flåtten, T. and Munkejord, S. T. *Numerical resolution of CO_2 transport dynamics*. SIAM Conference on Mathematics for Industry: Challenges and Frontiers (MI09), San Francisco, CA, USA, October 9-10 (2009).

[8] Munkejord, S. T. *Analysis of the two-fluid model and the drift-flux model for numerical calculation of two-phase flow*. Doctoral Theses at NTNU, 2005.

[9] Munkejord, S. T., et al. *Thermo- and fluid-dynamical modelling of two-phase multi-component carbon dioxide mixtures*. Int. J. Greenhouse Gas Control (2010). DOI: 10.1016/j.ijggc.2010.02.003.

[10] Munkejord, S. T., Evje, S. and Flåtten, T. *The multi-stage centred-scheme approach applied to a drift-flux two-phase flow model*. Int. J. Numer. Meth. Fluids 2006; **52**: 679-705.

[11] Munkejord, S. T., Evje, S. and Flåtten, T. *A musta scheme for a non-conservative two-fluid model*. SIAM J. Sci. Comput., Vol. 31, No. 4, pp. 2587-2622.

[12] Toro, E. F. *Riemann Solvers and Numerical Methods for Fluid Dynamics. A practical introduction*. 2nd Edition. Springer, 1999.

[13] Toumi, I. *An upwind numerical method for two-fluid two-phase flow models.* Nuclear Science and Engineering: **123**, 147-168 (1996).